Design of a Portable Pneumatic Exosuit for Knee Extension Assistance with Gait Sensing using Fabric-based Inflatable Insole Sensors

by

Souvik Poddar

A Thesis Presented in Partial Fulfillment
of the Requirements for the Degree
Master of Science

Approved March 2020 by the
Graduate Supervisory Committee:

Wenlong Zhang, Chair
Hyunglae Lee
Hamidreza Marvi

ARIZONA STATE UNIVERSITY

May 2020

ABSTRACT

Current exosuit technologies utilizing soft inflatable actuators for gait assistance have drawbacks of having slow dynamics and limited portability. The first part of this thesis focuses on addressing the aforementioned issues by using inflatable actuator composites (IAC) and a portable pneumatic source. Design, fabrication and finite element modeling of the IAC are presented. Volume optimization of the IAC is done by varying its internal volume using finite element methods. A portable air source for use in pneumatically actuated wearable devices is also presented. Evaluation of the system is carried out by analyzing its maximum pressure and flow output. Electro-pneumatic setup, design and fabrication of the developed air source are also shown. To provide assistance to the user using the exosuit in appropriate gait phases, a gait detection system is needed. In the second part of this thesis, a gait sensing system utilizing soft fabric based inflatable sensors embedded in a silicone based shoe insole is developed. Design, fabrication and mechanical characterization of the soft gait detection sensors are given. In addition, integration of the sensors, each capable of measuring loads of 700N in a silicone based shoe insole is also shown along with its possible application in detection of various gait phases. Finally, a possible integration of the actuators, air source and gait detection shoes in making of a portable soft exosuit for knee assistance is given.

DEDICATION

Dedicated to my family and Shilpashree for their unconditional love, care and support.

Also dedicated to my sweet Puto.

ACKNOWLEDGMENTS

I wholeheartedly thank my advisor, Dr. Wenlong Zhang for his support throughout the process of working on my thesis and helping me out during my hard times. I thank Dr. Hyunglae Lee and Dr. Hamidreza Marvi for taking their valuable time out from their busy schedules to provide me valuable feedback for my work. My never ending gratitude goes to my PhD seniors Saivimal Sridar, Pham Huy Nguyen, Zhi Qiao and Sunny Amatya for their unconditional help and support throughout my stay in lab since Fall 2018. Without their love and cooperation, it would have been impossible to finish my thesis work. I would also like to express my gratitude to the other members of Robotics and Intelligent Systems Laboratory for being great lab mates and making the lab atmosphere fun, friendly and an ideal place to work and gain knowledge.

Finally, I would like to thank Arizona State University for funding my research through Master's Opportunity for Research in Engineering fellowship for Fall 2019 and Spring 2020 semesters.

CONTENTS

LIST OF TABLES

Table Page

LIST OF FIGURES

Figure Page

Chapter 1

INTRODUCTION

1.1 Background and Motivation

Stroke afflicted population in the United States approximates over 795,000 per year [1]. Lower-limb muscular inactivity is a very common consequence among stroke survivors which result in abnormal gait patterns [2, 3]. This results in high energy cost of walking while a patient tries to compensate for the abnormal walking patterns. Such behaviors happen mainly due to loss in motor function in various parts of the brain which are associated with controlling the lower limbs. Therefore, to regain motor abilities, physical rehabilitation is essential [4], and its goal is to help the patient in relearning the lost muscular functions by performing several repetitive tasks. However, work loads on physical therapists have dramatically increased over the past years with the increase in demand for physical rehabilitation [5]. To reduce the workload on physical therapists, assist generated from robotic devices can be a viable option [6].

Current robotic rehabilitative devices for the lower extremity are mainly rigid and they suffer from limitations of being bulky and having less portability [7, 8, 9]. They utilize the assistance provided by motor [10], spring damper systems [11, 12] and hydraulic cylinders [13, 14] for providing the extra assistance. Therefore, there is a need for lightweight portable devices which can provide lower-limb assistance [15, 16, 17]. Gait feedback is very much essential for working of such devices. Keeping such requirements in mind, the forthcoming sections are going to talk about existing

soft exosuit technologies, portable pneumatic sources and the current gait sensing methodologies.

1.2 Soft Exosuits

Given the drawbacks of rigid exoskeletons, many efforts have been put to make the system lightweight by using soft robotic actuators instead of motors, springs and cylinders. Soft actuators have a lot of advantages over their rigid counterparts because of being lightweight, compliant, low-cost, and easy to fabricate. Current exosuits utilizing soft actuators are mainly cable-driven [18, 19, 20], fabric-based [21, 22, 23] or elastomeric [24, 25, 26]. Even though all the aforementioned actuators have been tested for rehabilitation of both extremities, there is a significant void in research in the use of fabric based actuators for the lower body. Some well-known use of fabric-based actuators for lower limb rehabilitation are [22, 23]. In these works, inflatable actuators were used which consists of heat sealed thermoplastic polyurethane (TPU) layers encased in nylon fabric. Inflation of the TPU layers generated the extra torque which gave knee extension assistance. Evaluation was conducted through electromyography (EMG) analysis showing significant reductions in muscle activity of various muscle groups with the exosuit powered on. However, inflatable actuators have slow dynamics because of its high internal volume. Therefore, this work focuses on using inflatable actuator composites which employs rigid paddles in conjunction with inflatable fabric layers, thus, reducing the inflation volume. The advantage of using actuator composites is that by reducing the internal volume, faster dynamics can be achieved. In this work, the fabric based inflatable beams (IFB) used in earlier works [22, 23] are compared with their inflatable actuator composite (IAC) counterparts by

measuring deflection performance when subjected to an externally applied load with change in internal pressure. Furthermore, to perform design and volume optimizations of the actuator composite, finite element models (FEM) of IFB and IAC are developed and validated with experimental results. Finally, FEM optimization of internal volume of the actuator composite is carried out.

1.3 Portable Pneumatic Sources

Even though considerable efforts have been made in making portable pneumatic sources for mobile robotic applications, its usage in wearable devices is limited. Current compressors are generally battery-powered micro-compressors or use the emission generated from compressed fluid and direct chemical reactions [27]. For high pressure and flow outputs, CO_2 cylinders and combustion methods are recommended [27]. Dry ice as a fuel was utilized in powering a lower-limb exoskeleton in a previous work but it would need replacement of the power cell after use [28]. A hybrid pneumatic source combining phase change of CO_2 and DME (Dimethyl Ether) was proposed in an earlier work which used the high pressure generation capability of CO_2 and high flow output capability of DME to have combined high pressure and flow output [29]. However, it suffered from the same limitation of requiring continuous replacement of the vessel for refilling purposes. With the limitations in using the aforementioned methods in portability scenarios, limited work used crank shafts, DC motors and portable air tanks for generating pneumatic output. One well-known portable exosuit developed by Havard Biodesign group used a back pack mounted frame consisting of air tanks, pneumatic valves and other control components to power a Mckibben actuator [30]. A similar work was done recently in [31] where air tank was used to power pneumatic

gel muscles. However, both of them required the air tank to be recharged by an external compressor prior to use. The weight of the overall system developed by Havard Biodesign group was also very high (9.1 kgs). To address the aforementioned issues, use of motor and crankshafts were explored in several works. One such work employed eight piston cylinder arrangement, placed in a radial fashion to make a mobile compressor [32]. Even though the system is suitable for potential use as a portable air source, the overall volume of the system will be too high when integrated with other control components. A recent work by Kim et al. [33] has shown use of a mobile light weight microcompressor utilizing double piston crank arrangement for powering a wearable robot. The system has the capability to produce a pressure output of 0.986 MPa and a flow rate of 9.78 SLPM. However, wearable devices need higher flow rate for operation. Previous soft exosuits utilizing fabric-based actuators operated at a pressure and flow output of 0.027 MPa and 20 SLPM, respectively. Therefore, keeping in mind the functional requirements of an ideal pneumatic source to be used in a fabric based inflatable exosuit, a new design of a portable air source is proposed in this work. Fabrication and control components of the system are explored. Furthermore, pressure and flow characteristics of the air compressor are also determined.

1.4 Gait Detection

Gait sensing is necessary to control wearable devices in providing assistance to the user at different gait phases. For rehabilitation purposes in particular, a controller would need the measurement of human gait kinematics to assist the user as and when needed through the wearable device. A common approach for gait sensing is to embed

sensors in shoe insoles. Insole sensors can be classified into different forms based on their working principles namely, resistive, capacitive, inductive, fiber bragg grating and pneumatic sensing. The next subsections are going to give a brief review about the existing works in each of the above working principles used in insole sensing.

1.4.1 Resistive Insole Sensing

The most commonly used insole sensors in current literature are force sensitive resistors (FSRs) [34]. These sensors use the principle of change in electrical resistance due to an externally applied pressure. Generally, FSRs are placed in the pressure sensitive areas of the insole so that the resistance change of all the insole sensors can be calibrated to give the ground contact force measurement. Other resistive sensors include optoelectronic sensors which have been used by Rossi et al. [35, 36]. In optoelectronic sensing, an LED and a photodiode are encased in an opaque silicone casing. Deformation of the opaque silicone lowers a silicone curtain, thus obstructing the light density received by the photodiode from the LED. This causes change in output voltage of the photodiode which can be calibrated with the external deformation force. A total of 64 such sensors were integrated in a shoe insole to detect the plantar pressure. However, such resistive sensors are prone to mechanical failures after prolonged and repetitive usage. Also, the FSRs mentioned above are not accurate for measuring the Ground Contact Force (GCF). Resistive properties of conductive fabrics have also been explored in earlier works. For detecting plantar pressure, such fabrics were coated with silicone rubber for making it resistant to moisture and dust [37]. In another work, a fabric based insole sensor was fabricated which consisted of piezoresistive and conductive materials enclosed within layers of Polyvinyl chloride

(PVC) [38]. The working principle of such sensor is that as conductive carbon filler particles come close to each other during deformation, a change in electrical resistance is obtained. Use of multi-walled carbon nanotubes (MWCNTs) have also been explored for use in plantar pressure detection [39]. In this type of sensing mechanism, MWCNTs are uniformly dispersed inside polydimethylsiloxane (PDMS) casing. Deformation of PDMS layer brings the MWCNTs closer to each other, increasing the number of conductive paths and a consequent decrease in resistance. Other resistive sensing mechanisms include liquid sensing strain sensors which uses ethylene glycol liquid injected into porous elastic rope/elastomer matrix (PER/EM) composite structure to obtain a liquid-impregnated porous elastic rope (LIPER) which is in turn embedded in a flexible silicone matrix [40]. Use of polyamide tubes have also been shown for potential use in resistive insole sensing [41]. Direct laser writing carbonization have been used to engrave various patterns in the walls of the PI tubes for various sensing purposes. Such tubes can be enclosed in PDMS for use in gait sensing.

1.4.2 Capacitive Insole Sensing

Capacitive sensing has a lot of advantages over resistive sensing, including less hysteresis as well as improved stability and precision. Capacitive sensors are layers of conductive electrodes enclosing a layer of dielectric. External force causes the thickness of the dielectric layer to change and a change in the value of capacitance is obtained. One application of capacitance sensing used in earlier work is shown in [42]. The sensor consisted of four layers of copper electrodes and a dielectric layer. Eight of these sensors were embedded in each insole for identifying different gait phases. iCub skin is a famous application of tactile capacitive sensing used in insoles which is an

array of 12 PCBs containing capacitive sensors out of which ten are used for pressure sensing and two for temperature compensation [43]. Other uses of capacitive sensing are piezoelectric transducers which appear in the form of ceramic disks and are much cheaper than resistive FSRs [44]. While fabric-based resistive insole sensing has been explored in earlier literature, capacitive properties of such fabric sensors were also utilized for use in sensing. One such work used layers of cotton cloth and conductive silver cloth to make a capacitive sensor [45]. Use of textile-based capacitive sensing was mentioned in a work done by Wang et al. [46]. Other forms of capacitive sensing include use of polyvinylidene fluoride (PVDF) layer as dielectric between layers of aluminum electrodes [47]. Use of pores based soft composite made of liquid metal alloy and Ecoflex-0030 has also been used for energy harvesting and force measurement utilizing capacitive principle in earlier works [48].

1.4.3 Inductive Insole Sensing

The last sections talked about few previous works utilizing etextiles for use in resistive and capacitive sensing. However, they suffer from certain disadvantages of having signal fluctuations and complex wiring. Therefore, a recent work introduced inductive etextile based insole sensing [49]. It consists of a (Inductor- Capacitor) LC antenna and thin ferrite film encasing a fabric spacer. When external pressure is applied on the sensor, the fabric spacer gets compressed which in turn reduces the distance between the LC antenna and ferrite films. This results in a change in the resonant frequencies of the LC antennas and a consequent change in inductance value.

1.4.4 Fiber- Bragg Grating Insole Sensing

Fiber bragg grating technique works on the principle of analyzing a specific light ray called bragg's wavelength [50]. When an induced light falls on bragg grating section of an optical fiber, one ray of light gets transmitted and another one gets reflected back. Wavelength of the reflected ray is termed as bragg's wavelength. This wavelength is further analyzed to sense the deformations and external pressure. One primary disadvantage of using optical fiber is that it is expensive and hence, is not ideal for wide usage.

1.4.5 Soft Pneumatic Insole Sensing

This type of sensing generally uses coiled silicone tubings embedded in a shoe insole [51]. The tubings are placed in toe, heel, fourth and fifth metatarsophalangeal joints respectively. External deformation force on the tubings cause the internal pressure to change which is sensed by pressure sensors mounted on a sensor box. This pressure change is further mapped with the GCF. Gait events using the GCF can be identified by means of fuzzy logic [52]. Use of these type of insole sensors have been demonstrated in soft inflatable exosuit for knee extension applications [23]. The GCF data from the shoe was used to regulate the pressure inside the soft inflatable actuators to provide the required assistance according to the gait phase. Such sensors have high repeatability compared to FSRs. Limitations of using silicone tubings lie in having complex fabrication, need for re-calibration prior to use, and having rate dependent hysteresis.

Even though there are a large variety of gait sensing methods being used by

means of embedding sensors in shoe insoles in current literature, they have certain disadvantages for having complex fabrication methods, signal fluctuations and being expensive. This thesis introduces soft inflatable fabric based sensing to counter some of the aforementioned issues. Inflatable sensors were used in several earlier works to sense external deformation pressure. A work by Wang et al. [53] introduced force sensing utilizing two deformable chambers where one was used as an actuator and the other one was used as a mechanoreceptor. Difference in air pressure of the two chambers was used to sense deformation and the force value was decoded by including system dynamics. A similar way of force sensing by using multiple chambers was done in another work by Gong et al. [54] where one chamber was enclosed and the other one was open to the atmosphere. Multi-axis force sensing was also carried out by using radially symmetric pneumatic chambers [55]. Other than force sensing, efforts have been put in sensing curvature of objects as well. One such work used an inflation chamber and a sensing chamber for measuring both contact force and curvature of objects in gripping operations [56]. Other ways of sensing curvature include using optical waveguides and applying undeformable metal reflective coating on the inner walls of the pneumatic chamber [57]. Stretch of the sensor causes light loss emitted by an embedded LED which goes out through the micro cracks formed as a result of stretch. This light loss is sensed by a photo-diode which is embedded inside the chamber along with the LED. The principle of working is similar to optoelectronic sensors explored in previous sections. In addition to sensing curvature of objects, use of pneumatic sensors in detecting size of objects was also explored in [58]. In few works, instead of pressure sensing, change in pneumatic flow due to deformation in inflatable balloons was used to measure contact force and also the point of application of contact force as shown in [59].

Even though inflatable chambers have been used in pressure and force sensing in a lot of prior works, integration of such sensors in shoe insole and its use in gait sensing is challenging. This is primarily because of its possibility of air leakage due to external deformations and also, embedding the electro-pneumatic setup in shoe insole which includes pressure sensors, pneumatic valves and other control components. Since, the size of insole sensors should be small enough for embedding in insole, fabrication and design of such inflatable chambers which can bear the whole body weight of an individual, needs to be explored. Therefore, this work introduces fabric based inflatable chambers in insole sensing.

Chapter 2

INFLATABLE ACTUATOR COMPOSITE

As mentioned in earlier sections, the inspiration behind the concept of using inflatable actuator composites for application in knee extension was to achieve faster dynamics and less inflation work. Therefore, to have faster dynamics or faster inflation and deflation rates, volume of the inflatable fabric beam actuators used in prior works of exosuits is reduced and the extra space is replaced by employing rigid paddles. The rigid paddles were fabricated by 3D printing methods using solid Polylactic acid (PLA) material. The forthcoming sections are going to further explore the actuator composites in terms of designing, fabrication and finite element modeling.

2.1 Design and Fabrication

The dimensions of the actuator composite were taken similar to its inflatable fabric beam counterpart as mentioned in earlier works. The inflatable volume of the actuator composite was taken to be 33 % of the total volume of IFB. This value was taken to ensure that the paddles doesn't touch other while the actuator is fully bent. In order to make space for the actuator to inflate, spherical arches were given to the rigid paddles. The fabric was sewn along the arch boundaries to hold it in place. A total of 4 paddles were used to make the actuator.

The fabrication of the actuator composite involved heat sealing layers of thermoplastic polyurethane (TPU) and encasing it by using nylon 40D fabric. The nylon fabric layers were then sewed to each other to house the TPU balloon inside it. After

that, the nylon fabric was sewed again along the edge boundaries of the rigid paddles. Finally, each pair of rigid paddles were bolted to each other to form the actuator composite (Fig. 1).

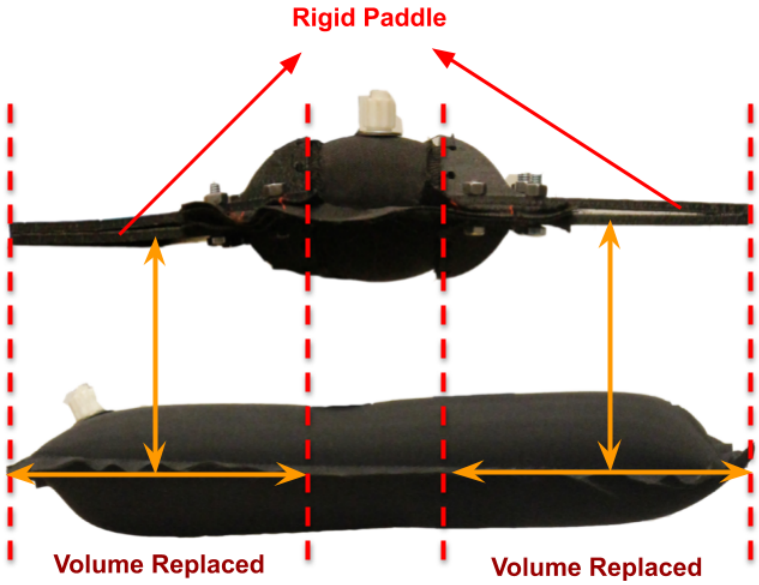

Figure 1: Overview Figure of IAC (Top) and IFB (Bottom)

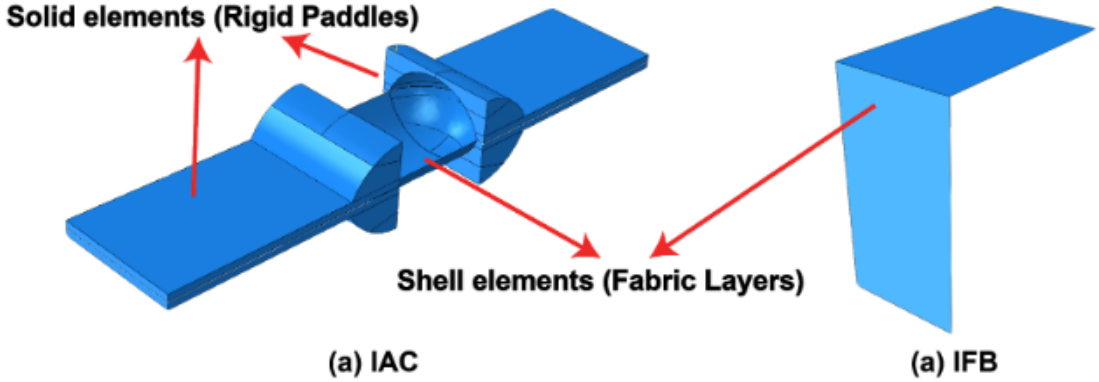

Figure 2: FEM Models for IAC and IFB

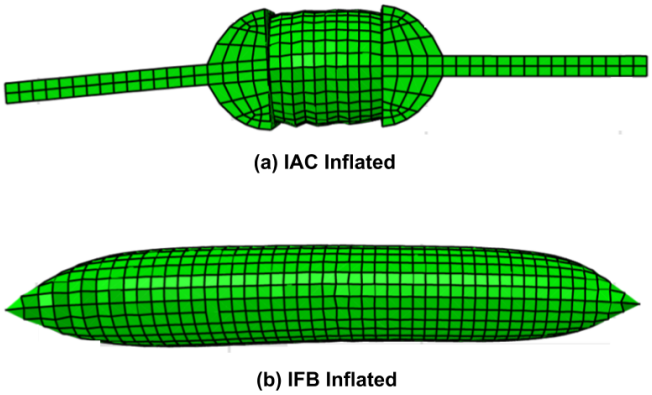

Figure 3: FEM Models for IAC and IFB (Inflated)

2.2 Finite Element Modeling

To perform computational modeling of the actuator for purposes such as design optimization, FEM was generated for both the inflatable fabric beam and the actuator composite. The FEM were built in Abaqus CAE software. For building the models, firstly CAD models were imported from Solidworks to Abaqus CAE in parasolid files due to the relative ease of generating complex CAD models in Solidworks. Tie constraints were used to create fixed contact between parts which are sewed and bolted in real time. After that, material characterization was done as per ASTM D882 test protocol to determine the young's modulus and poissons ratio for TPU (Young's Modulus of Elasticity = 5.1 MPa, Poisson's Ratio = 0.4) and Nylon 40D fabric (Young's Modulus of Elasticity = 728.22 MPa, Poisson's Ratio = 0.35). Polylactic acid (PLA) has an young's modulus of elasticity and poisson's ratio of 3600 MPa and 0.3 respectively. After the material properties of all the required parts were put into the software, the next step was to create and assign sections to all the parts. For

simulation purposes, the fabric layers were modeled as shell elements with 0.3 mm thickness and the paddles were modeled as solid elements (see figs. 2 and 3).

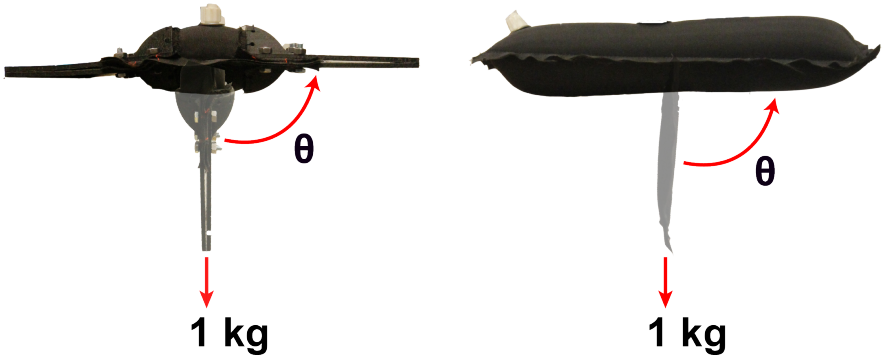

Figure 4: Deflection Test Experimental Setup

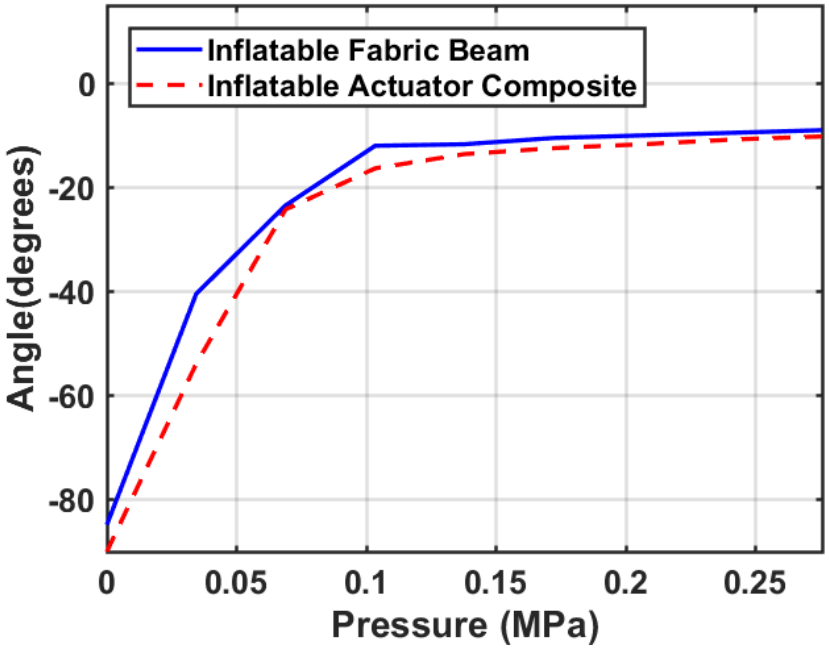

Figure 5: Experimental Results for Deflection Performance of IAC and IFB

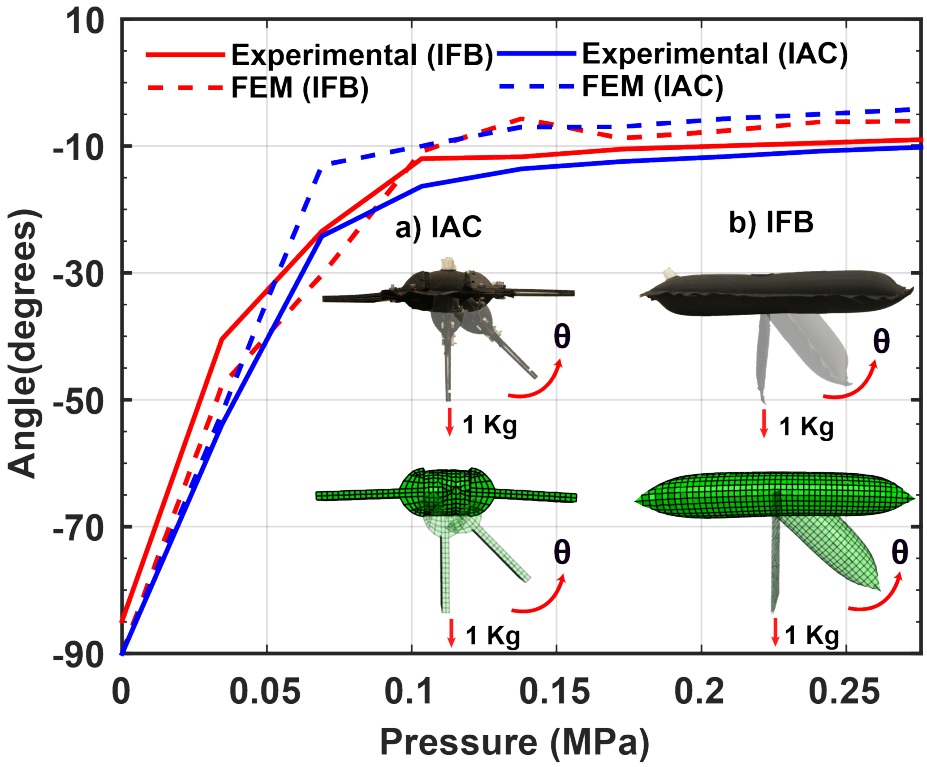

Figure 6: FEM Model Validations of IAC and IFB with Experimental Results

2.3 FEM Validation and Comparison with Inflatable Fabric Beam

In order to characterize the performance of the composite and the fabric beam, a deflection test was performed (Fig. 4). In this experiment, both the halves of the actuators and the mid point were fixed and subjected to a 1kg load at the free hanging end. The actuators were inflated in increments of 0.034 MPa to a maximum pressure of 0.276 MPa and the bending angle was recorded for each increment about the horizontal axis. It was found out that both the actuators exhibited similar performance characteristics even though the internal volume of the actuator beam was reduced (Fig. 5). To validate the finite element models generated for both the

actuator designs, they were simulated in various steps created in Abaqus CAE. To simulate the experimental setup in FEM, boundary conditions were used to fix the halves of the actuators and also that of the mid points. In place of the 1kg load, a concentrated force was applied at the edge vertices of the free hanging end. For the fabric beam, the actuator was designed in such a way that it already showed 90° deflection by default. Therefore the fabric beam was simulated in only one step by applying pressure load in a similar manner as was done for the experimental setup. A continuous gravity load was also given along with the concentrated force to account for the actuator weight. The FEM model of the IAC was simulated in two steps because of its complex geometry. For the IAC, 90° deflection was achieved by adding an additional step in the beginning which only includes the gravity load. Because of the complex structure of the composite, it was difficult to design it with a pre-90° deflection similar to the fabric beam.

It should be noted that the simulation was carried out in a quasi-static manner similar to the experimental procedure. Even though the system was simulated in a dynamic explicit environment, it was kept in mind that the values in parameter measurements are not affected by system dynamics. Dynamic Explicit in Abaqus has the capability of accelerating the simulation time by keeping the dynamics equilibrium in check in order to reduce the time required for computation. This is done by varying the loading rate and mass scaling factor in such a way that the kinetic energy of the system is not more than 5% of the total internal energy.

The data gathered through FEM simulation was further validated with experimental results (Fig. 6). The results showed that the values were very close with Root Mean Square Error (RMSE) of 4.63° and 6.33° for IFB and IAC, respectively. The

minor discrepancy in the values of FEM and experimental data is mainly due to errors in fabrication.

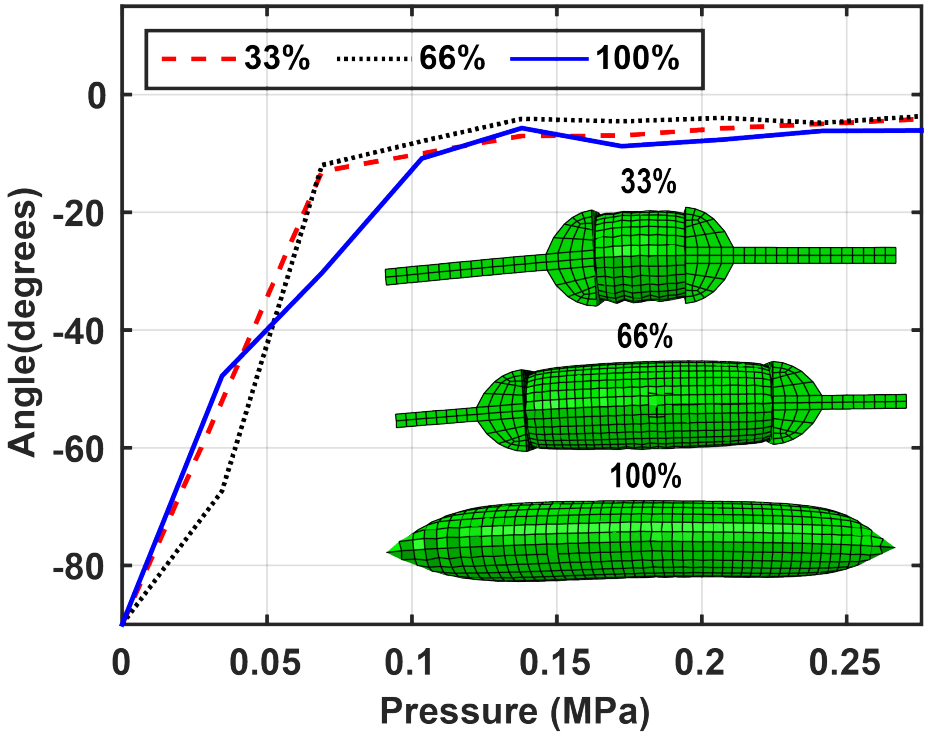

Figure 7: Volume Optimization of IAC by varying Internal Volumes

2.4 FEM Optimization

The previous sections talked about the design, fabrication and performance evaluation of the developed inflatable actuator composite. It was given that 33 percent inflatable volume section was chosen to ensure the paddles didn't touch each other while it was fully bent. It was also determined that the IAC had similar performance like IFB. However, comparing the performance of only two actuators gives little knowledge of predicting performance of composites with varying internal volumes.

In order to optimize the internal volume of the IAC, the composite was simulated with varying internal volumes at percentages of 33%, 66% and 100% (Fig. 7). The simulation was done in a similar manner as mentioned in the previous sections. The results follow similar profiles, thus concluding that the bending performance remains same with different internal volumes.

2.5 Strain Rates

In order to analyze the behaviour of the simulation, the material strain rates were plotted for all the steps for both fabric beam and composite. The strain rates plotted includes mechanical strain rate components (Fig. 8 and Fig. 9) and volumetric strain rates (Fig. 10). It is noted that here ER11, ER22 and ER33 represents the longitudinal strain rate components and ER12 represents the shear strain rate components.

The IFB shows significant increase in strain later than it shows for IAC. This is primarily due to the difference in scaling of X axis for both the plots. Therefore, even though the IFB starts showing significant strain rate increase after 0.1 seconds of simulation time, it is not visible in IAC plot because of the higher time scaling. From the plots it is clear that strain rates for IAC are less than IFB for both mechanical and volumetric strain rate components. This is due to the less inflation volume of the IAC.

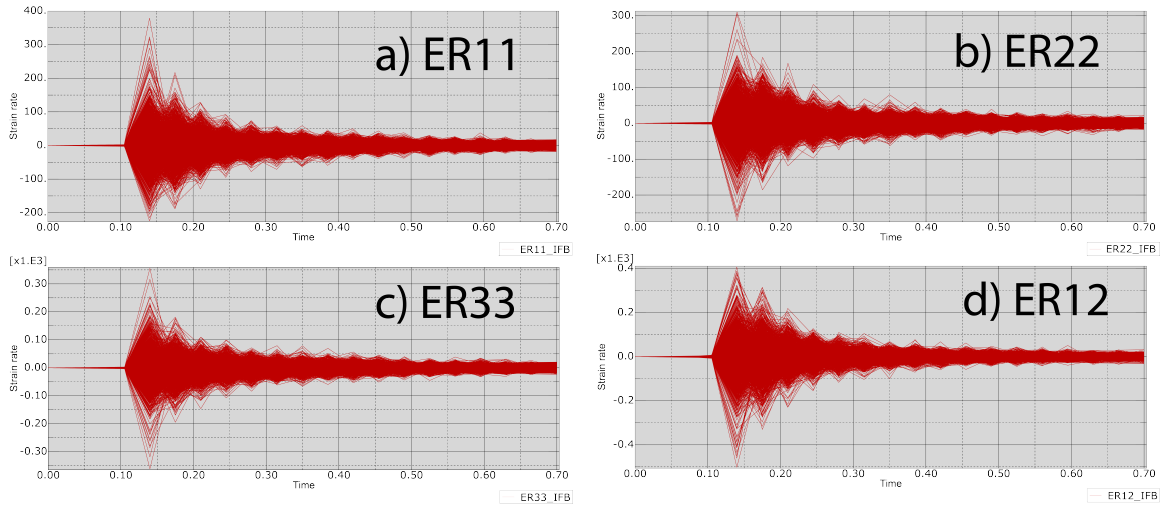

Figure 8: Mechanical Strain Rate Components for IFB

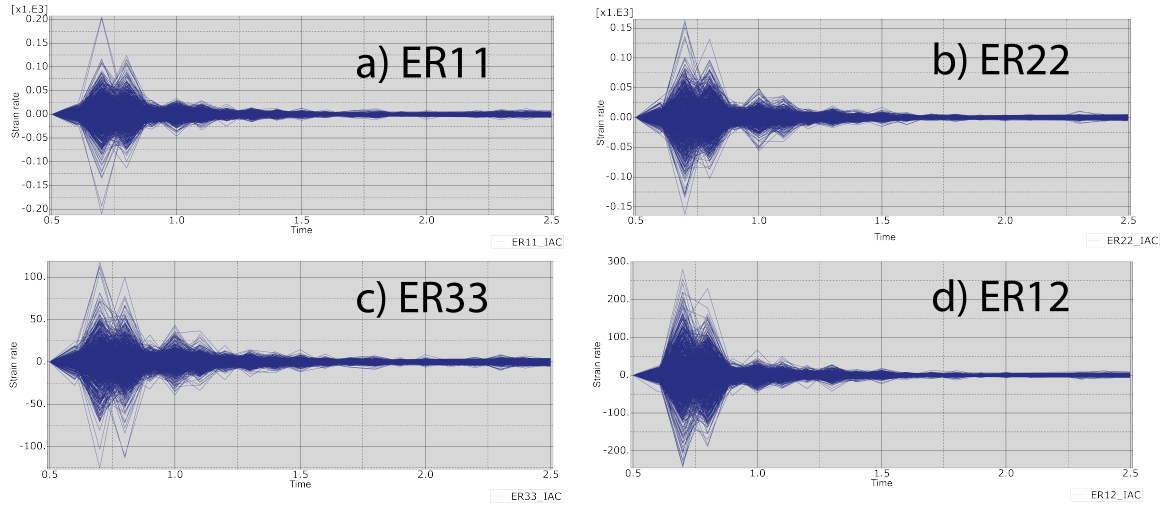

Figure 9: Mechanical Strain Rate Components for IAC

2.6 Force Characterization of Inflatable Actuator Composite

In order to characterize the performance of the IAC in terms of its force output, it was mounted on a 3D printed setup with movable links as shown in fig. 11. The setup was in turn mounted on an Universal Testing machine which has a pre-equipped load cell. The pressure was increased in increments of 0.034 MPa until 0.207 MPa and

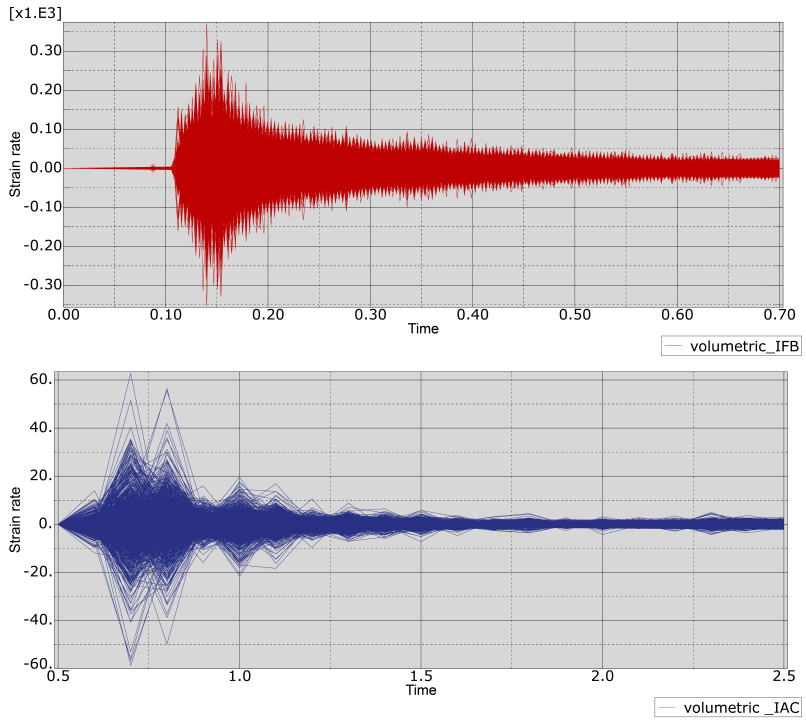

Figure 10: Volumetric Strain Rate Component for IFB (top) and IAC (bottom)

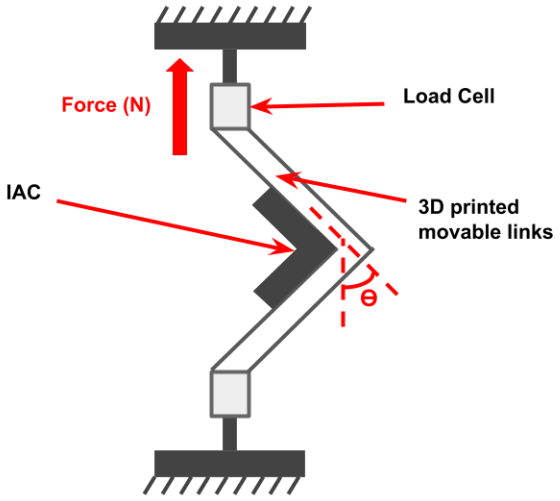

Figure 11: Experimental Setup for Force Characterization of IAC

the force output was noted from the load cell as the knee flexion angle was varied in angles of 45°,60°,75° and 90°. The force versus pressure characteristics of the IAC at

varied knee flexion angles is shown in fig. 12. It was found out that the force output of IAC increases with decrease in knee flexion angle.

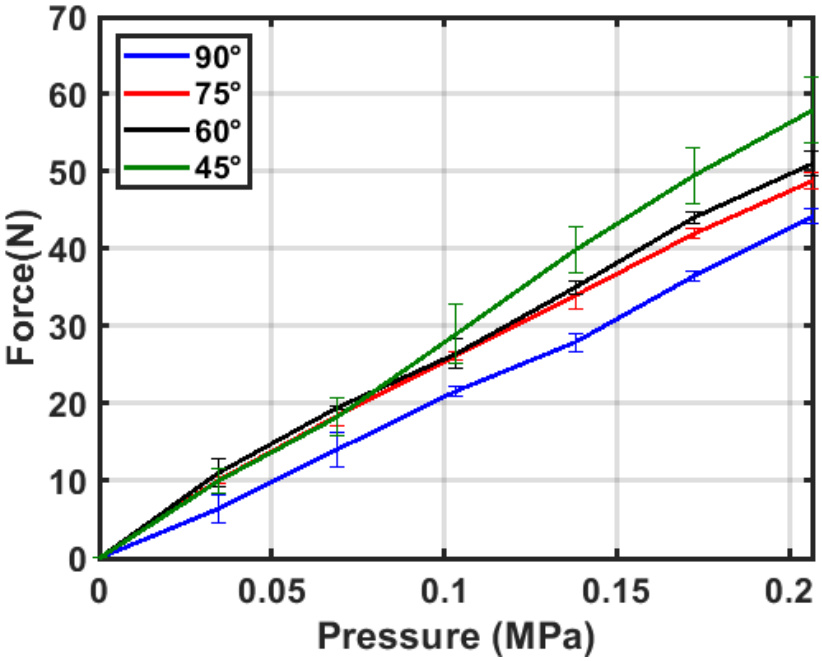

Figure 12: Force Characterization of IAC at varying Angles

Chapter 3

PORTABLE PNEUMATIC SOURCE

The previous sections talked about some of the drawbacks of current portable systems which are heavy, in need of frequent refilling and have low flow output. This work introduces a new design of an air source which is portable, have high flow output and doesn't need refilling unlike previous technologies. This system can be easily mounted on a back pack frame and can be used with any pneumatic wearable device which in our case is a knee exosuit. The functional requirements of the air source were set based on the previous version of the soft exosuit, utilizing fabric beam actuators which operated at a maximum pressure and flow output of 0.140 MPa and 20 standard litres per minute (SLPM) respectively. The dimensions of the portable system were taken similar to that of an ideal back frame on which the system can be mounted on which is less than or equal to 20cm×20cm×12.5cm. The coming sections are going to brief about the fabrication, electro-pneumatics setup and the performance evaluation of the air source.

3.1 Fabrication

The main driver of the portable air source is a high torque DC motor from amplflow (Amp-flow A23-150, 24V 10A). The DC motor when powered on, drove a pneumatic cylinder-piston arrangement back and forth via a lead screw mechanism, unlike using a crank shaft, as seen in previous portable air sources as mentioned in Chapter 1. The DC motor was fixed by means of 3D printed supports bolted to one another which

in turn was bolted to the system base which is an acrylic light weight board. The cylinder was threaded to a mounting bracket which was bolted to the acrylic base. All the components were arranged in a parallel fashion to reduce the height of the portable system. A rigid connector was 3D printed using Nylon material which acted as a connection between the lead screw and cylinder piston. A linear guide was used to support the connector which was mounted on shaft mounted supports at both ends. A flexible shaft coupler connected the motor shaft to the lead screw such that rotation of the DC motor shaft caused corresponding rotation of the lead screw. The overview of the system is shown in fig. 13. The entire system was mounted on a lightweight backpack frame such that it is portable and can be easily donned by the user as shown in fig. 14. The performance specifications of the pneumatic cylinder and DC motor used for fabrication are given below in Tables 1 and 2.

Table 1: Specifications of DC Motor

Voltage	24V
RPM	6400
Peak HP	0.9V
Weight (Pounds)	2.1
No Load Amps	1
Resistance (Ohms)	0.21
Efficiency	82%
Diameter	2.3 inches
Lenght	3.5 inches

Table 2: Specifications of Pneumatic Cylinder

Bore Size	1.25 inch
Stroke	2.5 inch
Acting	Double Acting
Mounting Style	Front Nose
Side Ported Rear Thread	Side Port

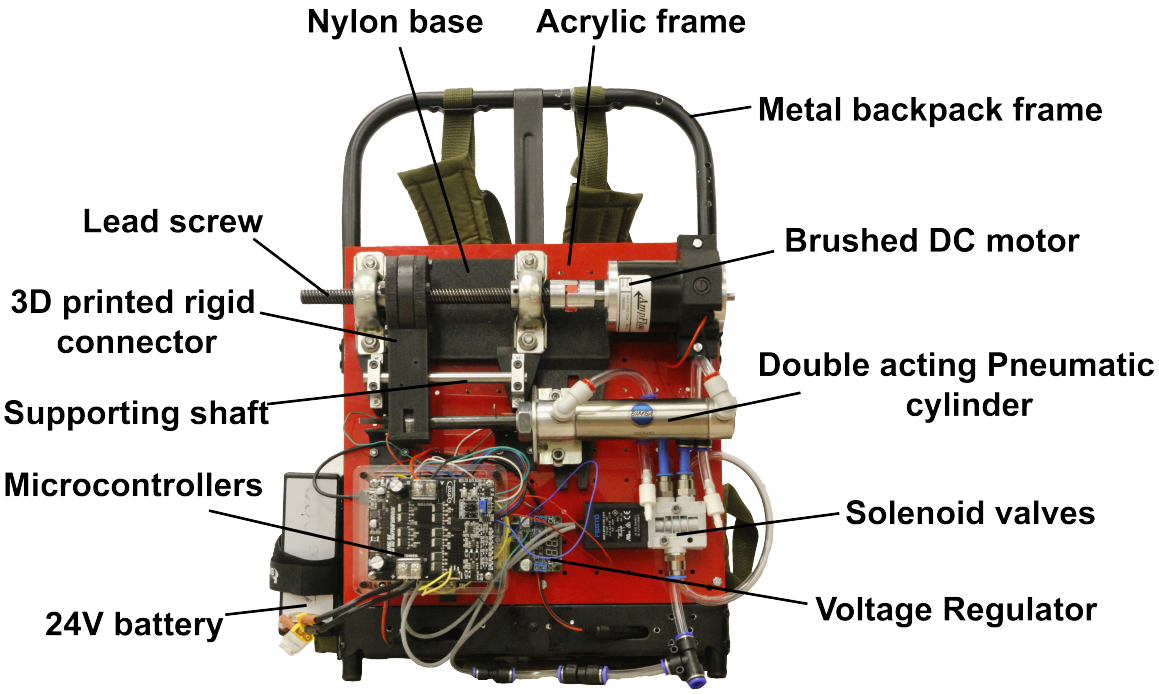

Figure 13: Portable Pneumatic Air Source

3.2 Electro-Pneumatics Setup

The electronic control circuitry of the system consists of a Raspberry Pi microcontroller and a brushed DC motor driver. The Raspberry Pi controlled the functioning of the whole portable system and the brushed motor controller controlled the direction of rotation of the DC motor as well as speed regulation via Pulse Width Modulation (PWM) signals. Limit switches were used to detect the completion of each stroke. Both limit switches were mounted on 3D printed supports bolted on both extremities of the piston shaft. As the connector touched the limit switches, it triggered the rotation of the DC motor in forward and reverse directions through the motor controller, depending on the direction of stroke. This change in rotation caused back and forth motion of the cylinder piston arrangement, thus generating pressurised output.

The pneumatic supply was obtained through fast switching solenoid valves which

Figure 14: Developed Air Source donned by a Human Subject

were controlled by a four-channel MOSFET board and one-way check valves. The solenoid valves were triggered with the change in rotation of the DC motor to create pressurised output through each consecutive stroke. A 24V Lithium Ion battery was used to supply power to the motor controller, Raspberry Pi and the MOSFET board. Since, the Raspberry Pi input voltage is limited to 5V, a voltage regulator board was

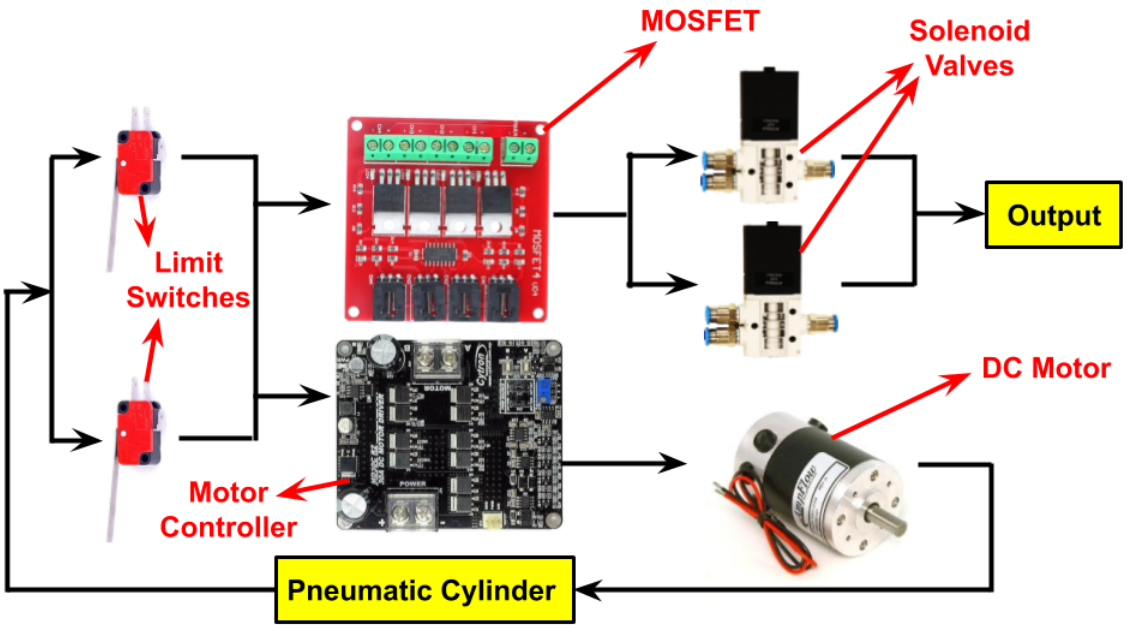

Figure 15: Electro- Pneumatics Setup

used to supply power to the Pi. All the motor controllers and the MOSFET board were bolted on transparent acrylic bases one above another. The 24V battery was mounted on the side of the back pack frame via Velco Straps. The schematic diagram of the working of electropneumatic control components in the air source is shown in fig. 15.

3.3 Performance Evaluation

In order to evaluate the performance of the developed portable pneumatic source, experimental tests were conducted in terms of its flow and pressure output generation capability.

For evaluation of pressure output, a pressure sensor (ASDXAVX100PGAA5, Honeywell International Inc., Morris Plains, NJ) was connected in series with the air flow

line connecting the portable source with the inflatable actuator composite via a three way plastic pneumatic connector. The maximum pressure was generated when the rotation of the dc motor stalled after few strokes and the value was noted. It was concluded that the maximum pressure the air source is capable of generating is 0.131 MPa when the flow output became zero after the dc motor stalled. The full pressure profile is also depicted as shown in fig. 16.

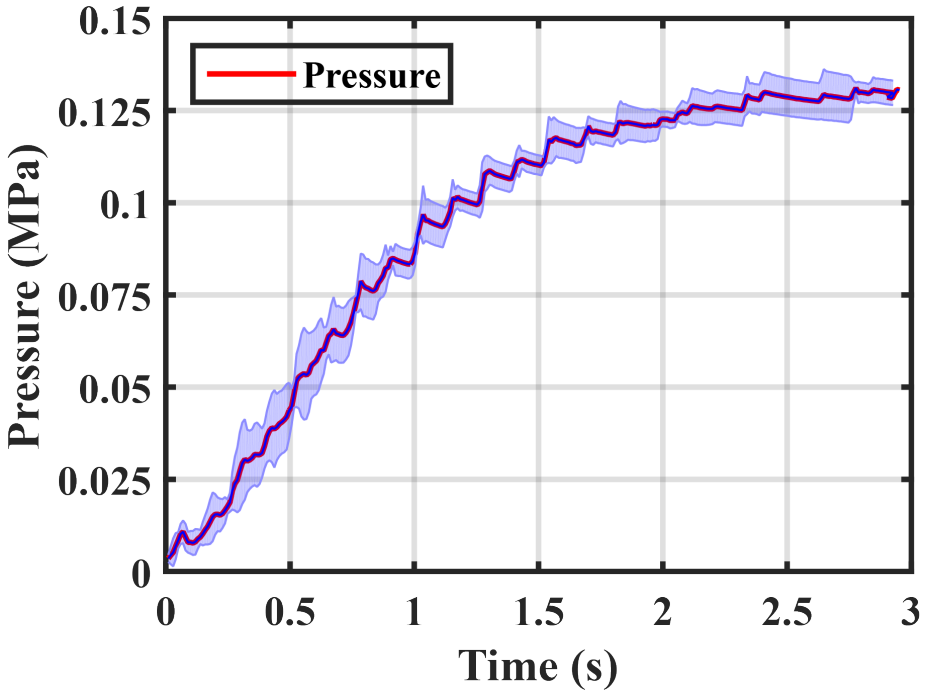

Figure 16: Pressure Evaluation Results

In order to evaluate the flow generation capability, an I2C flow sensor was connected to the output of the system coming out through the solenoid valves. It is noted that for this experiment, the actuator composite was not connected to the air source so that the DC motor didn't stall and multiple cycles of flow output could be generated going from minimum value to maximum value and vice versa. The maximum flow output noted was 21.45 SLPM and the whole profile is shown in fig. 17.

The total weight of the entire system including the back pack frame came out to be 5.1 kgs which is better than some previous portable sources [30].

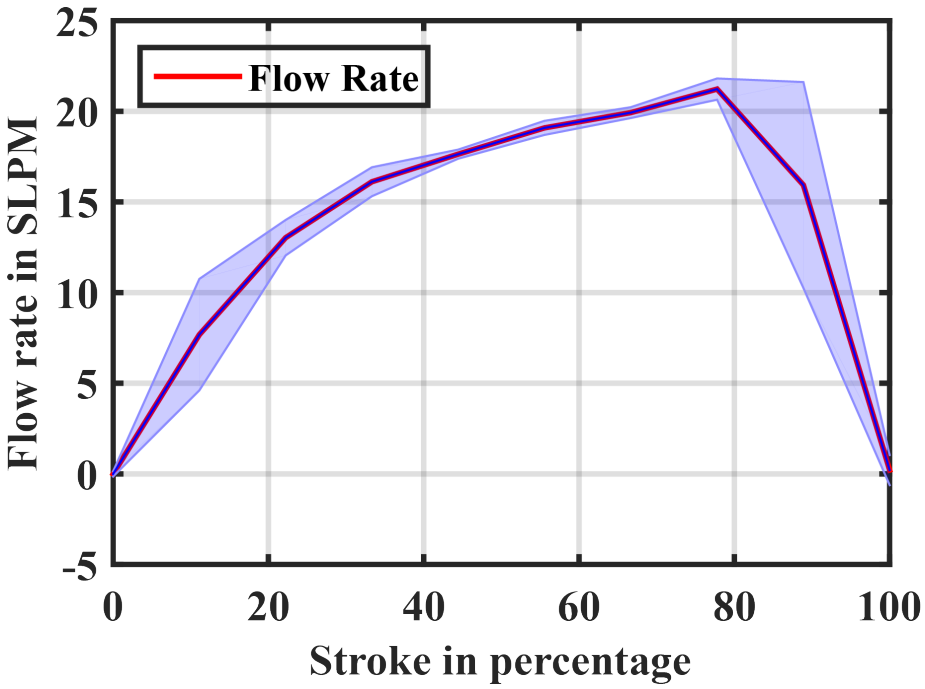

Figure 17: Flow Evaluation Results

Chapter 4

GAIT SENSING

This section talks about a novel way of gait sensing utilizing soft inflatable sensors embedded in a shoe insole. The upcoming sections are going to talk about the working of the inflatable soft sensor, sensor fabrication, design selection, details of mechanical characterization, insole fabrication and lastly, its use in gait detection.

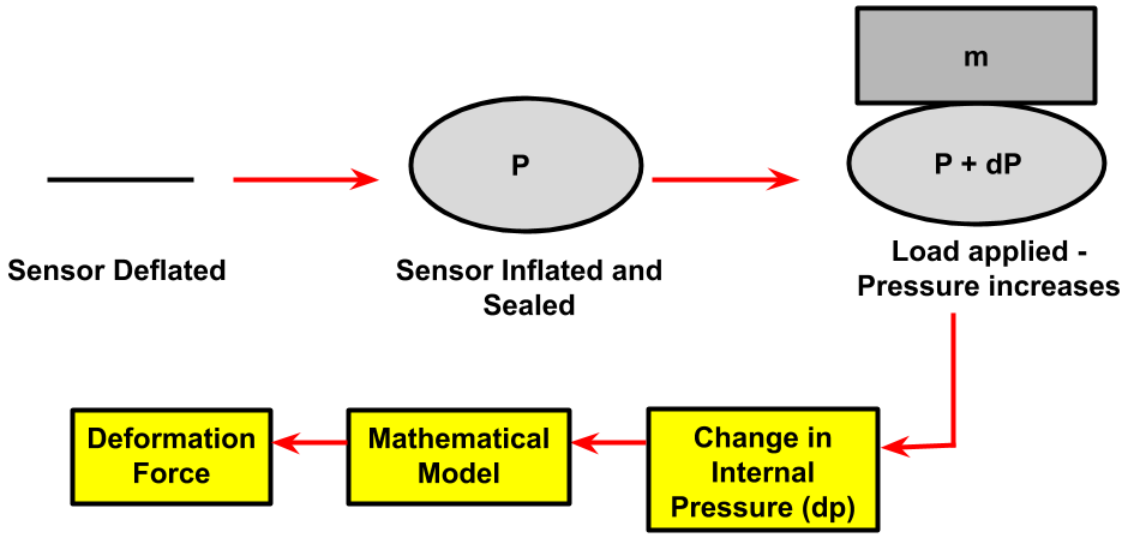

Figure 18: Working of Inflatable Sensor

4.1 Working of the Soft Inflatable Sensor

The working principle of the soft inflatable sensor is depicted in fig. 18. When the layers of the sensor are inflated at a certain pressure, it's volume increases and

becomes stiff. Now, when an external load is applied on the inflated sensor, a change in internal pressure will occur. This pressure change varies with the external deformation force, following a characteristic profile. When the pressure and deformation force are mapped, a mathematical model is obtained. This mathematical model is further used to get an idea of the value of the external deformation force corresponding to the change in internal pressure during compression.

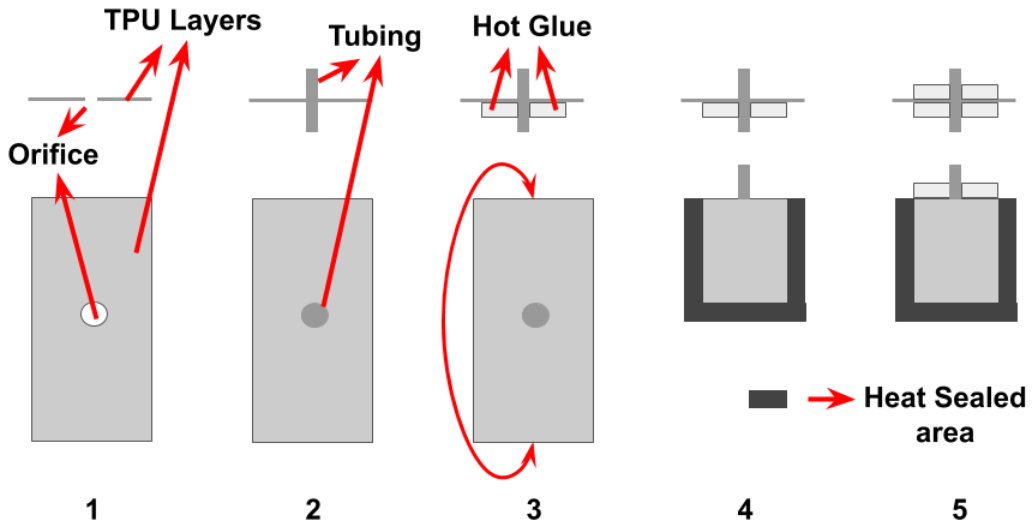

Figure 19: Sensor Fabrication Steps

4.2 Sensor Fabrication

The sensor was fabricated by using heat sealed thermoplastic polyurethane (TPU) layers encased in layers of Nylon Fabric, following the same procedures of fabrication as that of IFB and IAC. Since the heat sealed TPU layers fail at higher pressure because of their relatively low elasticity, they cannot be used for gait sensing which

would require high stiffness for sensing body weight. Therefore, they were housed inside layers of Nylon Fabric sewed to each other. Because of high elastic properties of nylon, they limit the stretchability of the TPU layers and hence, high stiffness is obtained. Previous works utilizing this concept of fabric based balloon fabrication used push-in threaded connectors which were bolted from inside of the balloon to provide air supply through plastic tubings [21, 60]. However, threaded connectors are not leak proof and can affect the repeatability of the sensors and a consequent deteoriation to the sensor accuracy in measuring loads for different gait cycles. This work shows a novel way of making leak proof sensors by eliminating the need for rigid connectors.

The fabrication methodology adopted in this work involved putting the tubings directly inside the sensor instead of using threaded connectors. At first, a single TPU layer was fabricated using laser cutting technologies which contained a small orifice in the center as shown in step 1 of fig. 19. A small piece of tubing was cut and a one way plastic connector was put inside of it. The tubing then went inside the orifice as shown in step 2 of fig. 19. After step 2, a layer of hot glue was applied around the tubing and the TPU layer was folded and heat sealed on three sides to make the TPU balloon such that the layer of glue faced inside the inflatable chamber as shown in step 3 and 4 of fig. 19. After the balloon was made, another layer of hot glue was put around the tubing on the other side of the TPU layer (step 5 of fig. 19). The TPU balloon was then put inside layers of Nylon fabric sewn to each other as shown in fig. 20. This method of fabrication is simple and eliminates the need for connector by directly putting the tubing inside the sensor. Moreover, this novel way of fabrication also eliminates the need for putting threaded nuts inside the sensor which would limit the extent to which the sensor can be deformed because the rigid nut consumes extra

space unlike tubing which is relatively smaller in size and compliant. Once the sensor was inflated, the air was held inside by means of one way check valves.

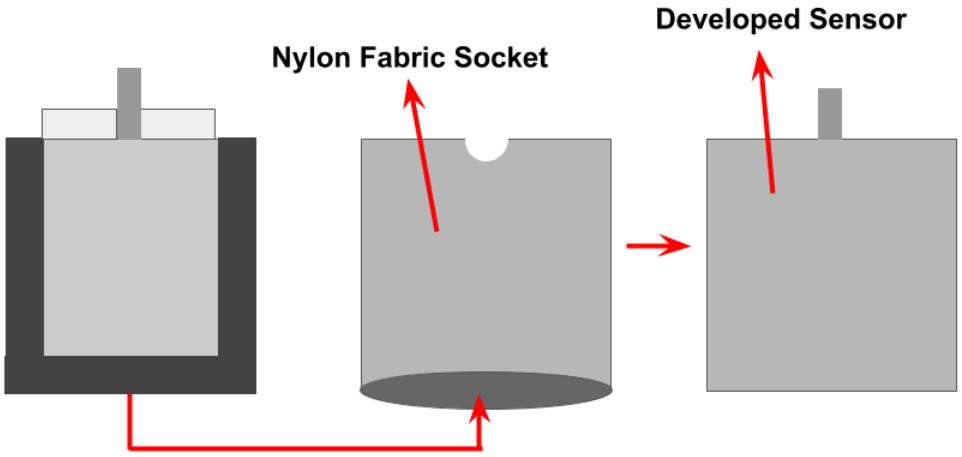

Figure 20: Placement of TPU Balloon inside Nylon Socket

4.3 Sensor Design

In order to determine the shape and dimension of the sensor, it is essential to list out the functional requirements for gait sensing. The functional requirements are listed in Table 3. The sensor is designed for the average weight of the entire population which is around 77kgs [61]. Since, during normal toe-off and heel strike, the force applied under the foot during walking is around 1.2 times the normal weight of an individual, it was estimated the average force applied under foot while walking is around 900N [61].

The maximum dimensions for the sensors were determined by taking a standard insole of size 9 and keeping some amount of clearance from the edges.

Table 3: Functional Requirements of Insole Sensing

Maximum Payload of each sensor	900 N
Average weight of person	77 kgs
Placement of sensors	Heel and Toe
Dimensions of each sensor	Less than 40mm × 40mm
Height of insole	Less than 15mm
Sensor Shape	Square or rectangle

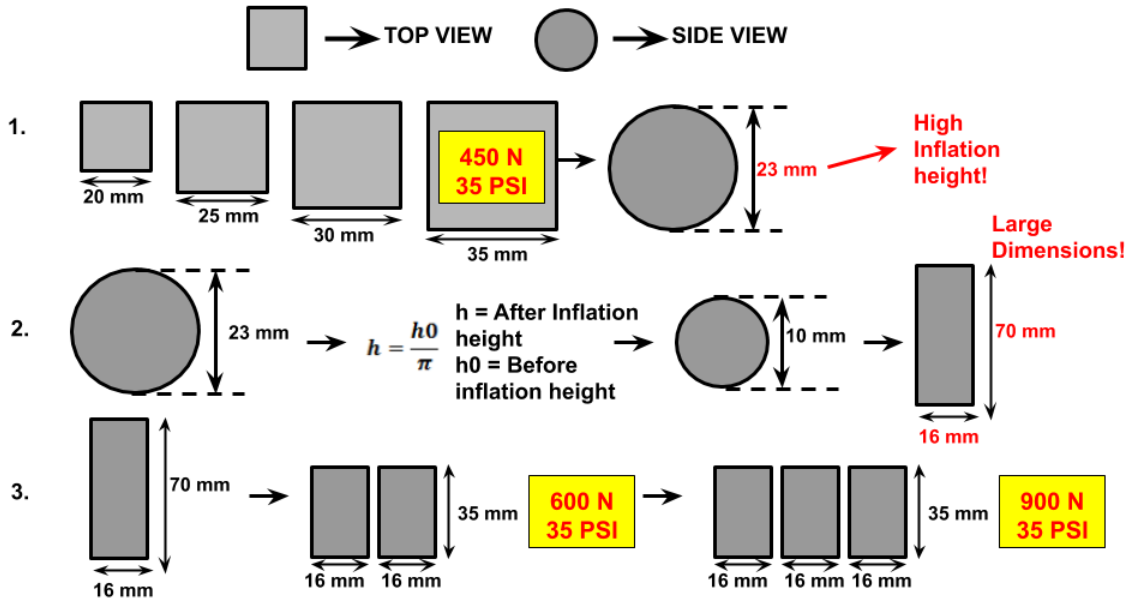

Figure 21: Sensor Design Selection Flowchart

The first step used in the design selection procedure (Fig. 21) was to fabricate four square sensors of dimensions 20m×20mm, 25mm×25mm, 30mm×30mm, 35mm×35mm and determine the performance of the sensors to get a baseline idea of the needed dimensions to get a sensor that can have 900N payload capacity. To

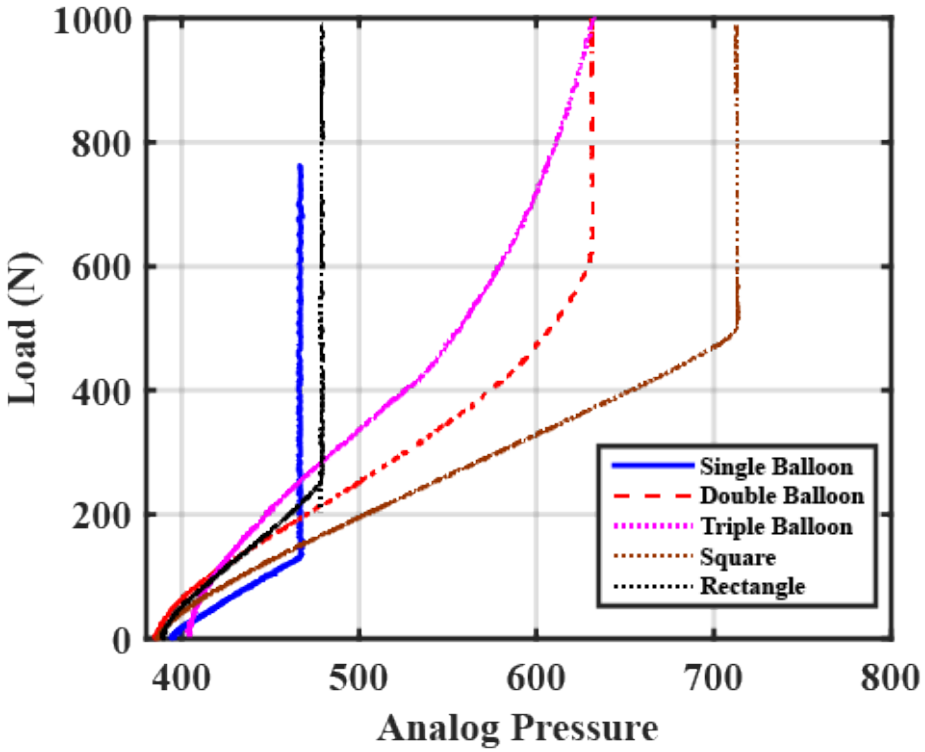

Figure 22: Sensor Design Optimization

characterize the performance of the sensors, all of them were inflated to a maximum pressure of 35 psi and mounted on an Universal Testing Machine (Instron 5944,Instron Corp., High Wycombe, United Kingdom). Compression testing was done at a slow speed of 10mm/min until the sensors were fully compressed. 35 psi pressure was chosen to limit the size of pressure sensors to be used for the application. It was found out that the square sensor of 35mm width could reach a load of 450N. The inflation height was also almost 23mm. According to the functional requirements for insole sensing, the maximum height should be less than 15mm. This value of 15mm was chosen by checking width of a standard insole which is around 10mm and then keeping some additional clearance for placement of sensors. Therefore, to reduce the inflation height to 10mm, a similar procedure was chosen to determine the inflatable balloon dimensions based on actual and desired inflation height as shown in [62]. By

calculation, the width of the sensor for desired inflation height of 10mm came out to be 17mm. In order to keep the volume same, the length of sensor was calculated to be 70mm. However, based on the functional requirements of insole sensing, such sensor dimensions are not feasible for placement in shoe insole. Therefore, to keep the volume same, the length of sensor was cut into half and two balloons were used, each of dimension 17mm×35mm.

However, the double balloon sensor can only reach 600N. To counter this issue, another balloon of similar dimensions was added. The triple balloon sensor could easily reach 900N as shown in fig. 22. Therefore, triple balloon sensor design is the best design that can be chosen for gait sensing applications (Fig. 23). The pressure output plotted here is the analog output of the pressure sensor which have a range of measurement of 0-100 psi. It is noted that for this plot and for all other plots, raw analog voltage output of the pressure senor has been chosen for plotting the pressure versus deformation force profiles instead of the calibrated value of the pressure output. This is because in future, this value of pressure will be used to get the value of external deformation force via a mathematical model. Therefore, it is necessary to map the pressure with deformation force using the raw analog voltage for achieving better accuracy. The length and width of the developed sensor after inflation were 35mm and 40mm respectively. The coming section is going to talk about the mechanical characterization of the sensor.

4.4 Mechanical Characterization

The mechanical characterization of the developed insole sensor has been categorized into different subsections based on the type of characterizations performed.

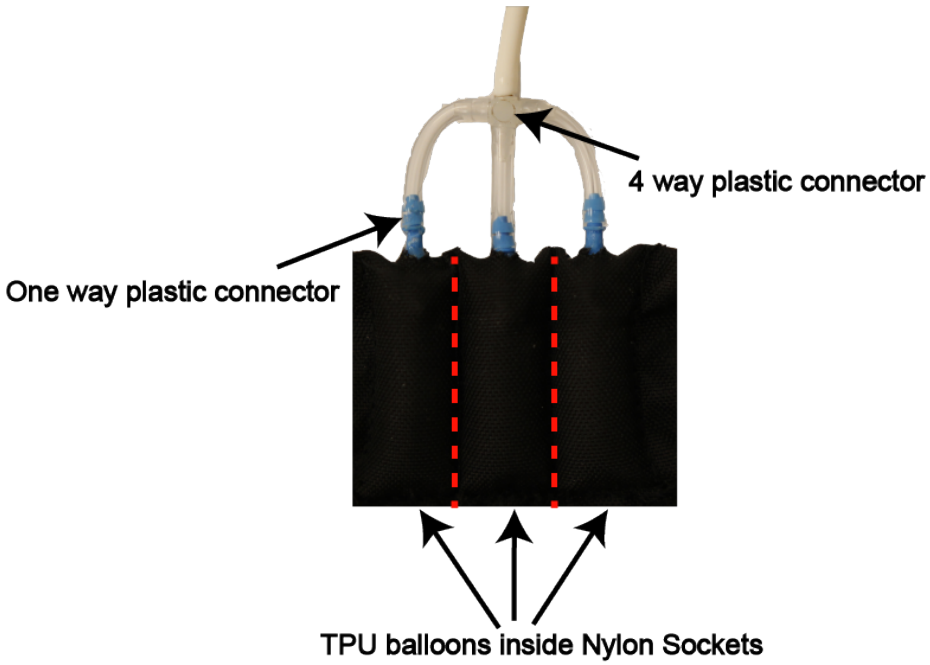

Figure 23: Triple Balloon Sensor

4.4.1 Load vs Deformation

The force versus deformation characteristics of the sensor is plotted as shown in the figure below (Fig. 24). The characteristic was obtained by performing compression test on an universal testing machine (Instron 5944,Instron Corp., High Wycombe,United Kingdom) at a speed of 10mm/min while the sensor was pre-inflated to a pressure of 35 psi. As it can be seen from the plot, the curve is of exponential type. Therefore, there exists a non linear relationship between force and inflation height as the sensor is compressed.

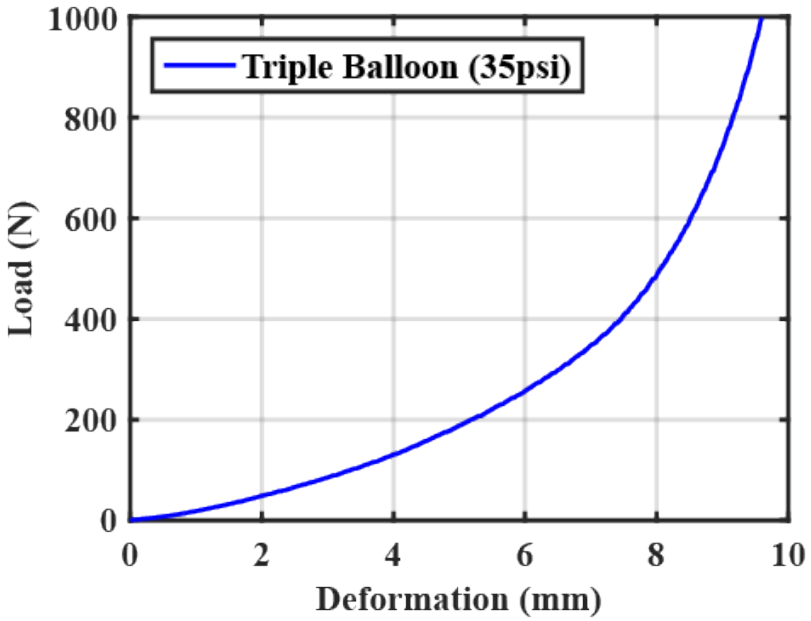

Figure 24: Load vs Deformation

4.4.2 Load vs Pressure

This characterization was done in a similar way as was done for load versus deformation experimental characterization (Fig. 25). Since, in future the pressure change due to external deformations will be mapped with the external load, the load was plotted in Y axis and the pressure in X axis. It can be seen from the graph that the profile shows a linear increase when compressed to some extent after which it starts increasing exponentially with a very high slope. The reason for this behaviour is explained. When the sensor was compressed initially, the cross section started decreasing and hence, there was an increase in pressure output. However, after some amount of compression, the cross section became flat and didn't show much change. It is from this point that the pressure became stagnant and didn't increase much, however, load continued to increase because of the ongoing compression and the sensor's stiffness. This point will be labeled as break point in the forthcoming sections.

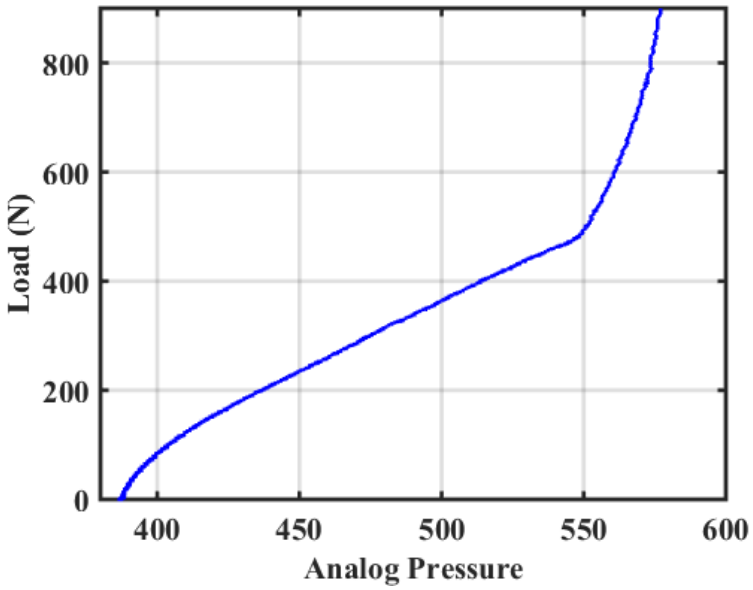

Figure 25: Load vs Pressure

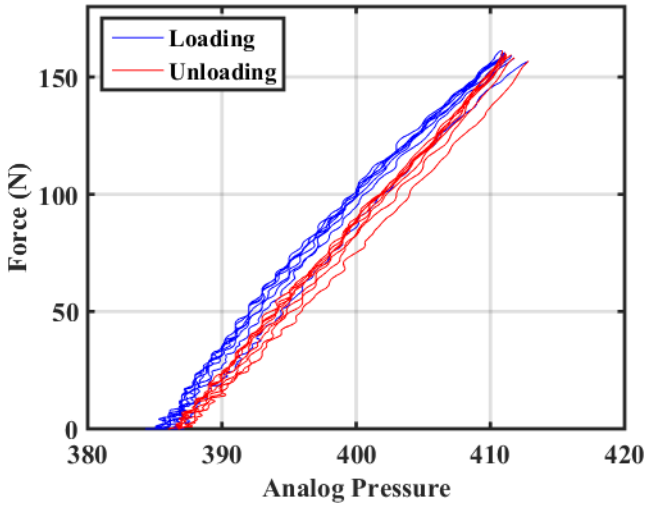

Figure 26: Hysteresis at Speed of 30mm/min

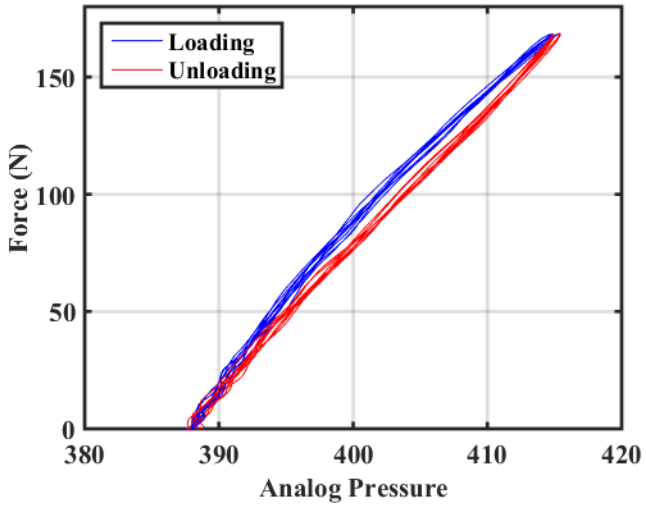

Figure 27: Hysteresis at Speed of 150mm/min

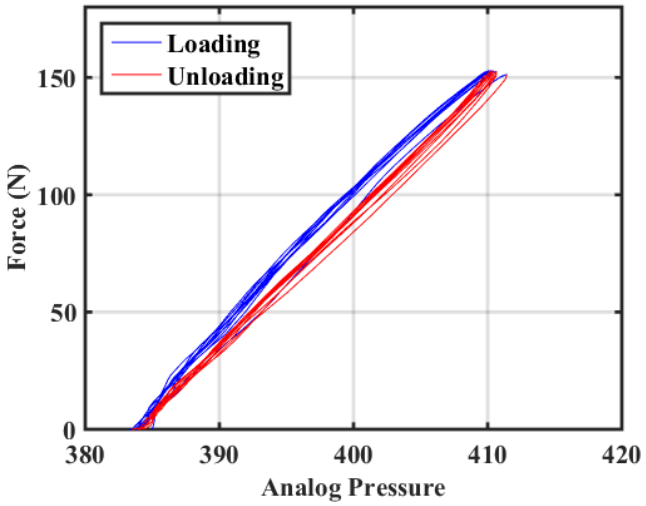

Figure 28: Hysteresis at Speed of 270mm/min

4.4.3 Hysteresis

In order to evaluate the dynamic lag between input and output, a cyclic loading test was performed. For this test, 12 cycles of loading and unloading was done as the sensor was compressed to half of the inflation width in the Universal Testing Machine

(Instron 5944,Instron Corp., High Wycombe,United Kingdom). Force versus pressure data was collected as the cyclic test was done at 30mm/min and plotted as shown.

The maximum hysteresis was calculated to be 10 percent of the maximum loading value. In order to determine whether this value of hysteresis is rate dependent or rate independent, the cyclic test was done at low speed (Fig. 26), medium speed (Fig. 27) and high speed (Fig. 28). It was found out that the value of hysteresis lied with 2 percent error range for the three loading rates. Therefore, the hysteresis of this sensor is considered rate independent which is an advantage if the sensor is used at higher speeds of walking.

4.4.4 Repeatability

Repeatability determines the ability of sensor to be used continuously for a prolonged period of time under similar environmental conditions. It is also an indication of how robust the sensor is. For testing the repeatibility, the pressure variation was mapped for multiple loading cycles following the same experimental procedure as was followed for testing hysteresis. It is noted that for repeatability test, the force was mapped to check if the sensor is leaking or not which would result in decrease of peak force value reached for each consecutive cycle. The data collected is plotted as shown with increasing sample number with variable speeds (Fig. 29, Fig. 30 and Fig. 31). The profile shows good agreement to a sensor with good repeatability with peak values for each cycle having standard deviations of 1.6 N, 1.1 N and 1.42 N at loading rates of 30 mm/min, 150 mm/min and 270 mm/min, respectively. This plot also validates the fact that the sensor is leak proof.

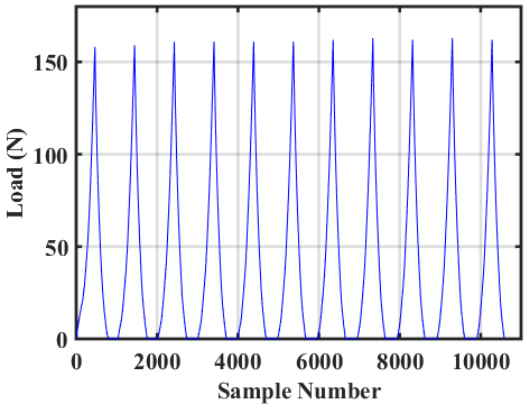

Figure 29: Repeatability at Speed of 30mm/min

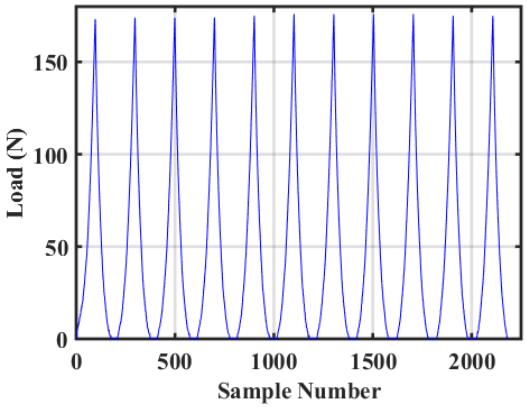

Figure 30: Repeatability at Speed of 150mm/min

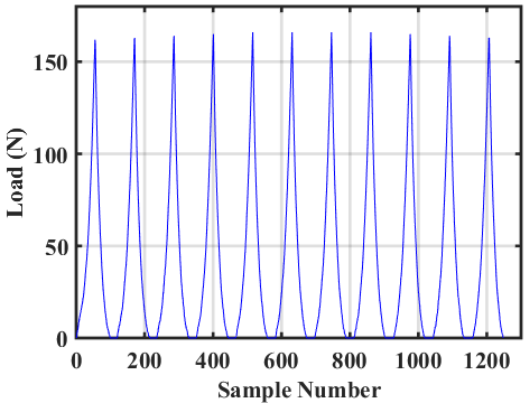

Figure 31: Repeatability at Speed of 270mm/min

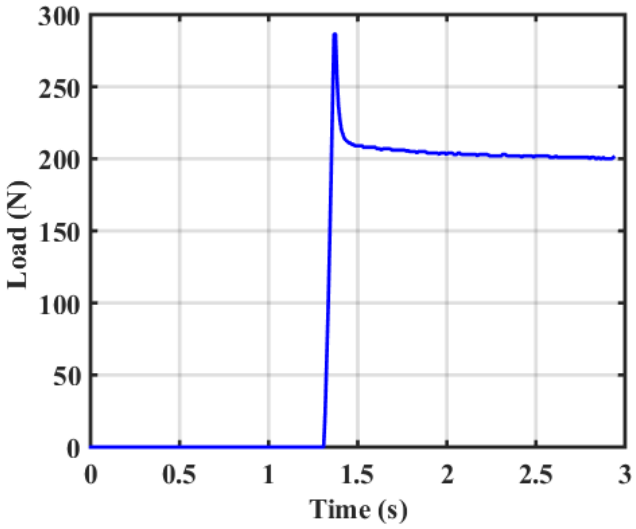

Figure 32: Step Response to Impact Loading

4.4.5 Step Response

In order to determine the stability of the sensor, a step response test was conducted. The Universal Testing Machine (Instron 5944,Instron Corp., High Wycombe,United Kingdom) was allowed to compress the sensor at a very high loading rate of 2000 mm/min until it reached 4 mm compression and was held in that position for some time. The sensor showed a good value of stability with a settling time of 0.946 seconds. The profile of the step response test is shown below in the figure below (Fig. 32).

4.4.6 Model Building and Performance Evaluation of Developed Model

Since, the main purpose of the sensor is to be applicable in gait sensing, a one to one mapping is required from the force versus pressure profile. The next step is to fit

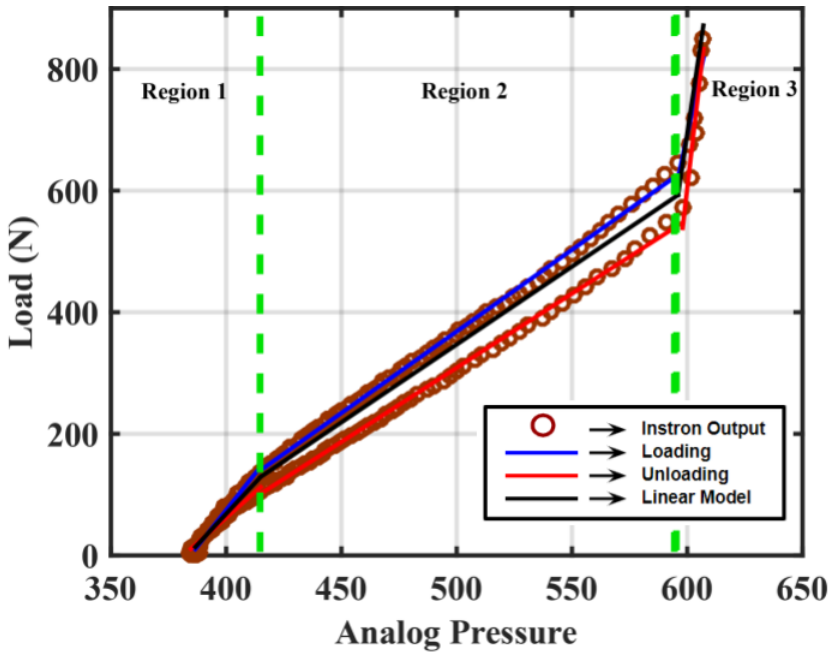

Figure 33: Model Building at 35psi

a model which can map the force correctly with change in pressure and generate the least amount of error. Furthermore, for GCF sensing, both loading and unloading curves must be considered. The force versus pressure profile for loading and unloading till 900N compression is shown in fig 33. This curve was obtained by doing a one cycle compression and relaxation test in an Universal Testing Machine at a high speed of 210mm/min which was chosen to approximate a normal walking speed. For model fitting, linear polynomial model of the form y = $m \times x$ + c was approximated using curve fitting tool Matlab which can generate the best fit according to the highest R^2 value. To start with the model building procedure, each of the loading and unloading curves were divided into three regions as shown in the fig. 33. Linear model having best R^2 value was chosen for each section for both loading scenarios. Due to the nature of the curves and also for ease of computation, linear model was used to approximate the curves instead of non-linear model. The model and its corresponding R^2 value

is tabulated as shown in table 4. After the three linear models were determined for both curves, mean of the fits were obtained for each section (table 5). Therefore, the model adopted for force mapping is a linear piece wise continuous function. The performance evaluation of the model was done by redoing the unloading and loading test in an Universal Testing Machine (Instron 5944,Instron Corp., High Wycombe, United Kingdom) using the similar compression and relaxation experimental setup as was done earlier (Fig. 34). Even though the model showed a good agreement with loading and unloading data, it can be seen that there are very less sample numbers in region 3. This is primarily because after the break point occured, the load increased very quickly within a short period of time. The reason for obtaining the break point was explained in section 4.4.2. This behaviour resulted in high error bar while using the sensor for sensing loads beyond the break point. Therefore, this model is a good model till 600 N which is the break point value and this means that it not ideal for measuring 900N load. Since, during toe-off, the maximum load can reach up to 1.2 times the actual body weight, the above model is ideal for a person having only 50 kg body weight.

To increase the value of the load after which the break point occurs, one possible way was to increase the internal pressure of the sensors so that it could have a better measuring range. For this purpose, the internal pressure was increased and the variation of the break point was noted. It was seen that the break point occured at at around 690N at an internal pressure of 55psi. 690N is ideal for a person weighing approximately 55 kgs. In order to increase the capacity of the sensor for measuring body weight of 77 kgs as per the functional requirements, the internal pressure needs to be higher than 55 psi. Keeping in mind the limitations of the size of pressure sensor to be embedded in shoe insoles, it was decided to optimize the sensor design instead

of increasing the internal pressure. To show the working capability of the sensor, the body weight of the individual that the sensor is designed for is restricted to 55 kgs within the scope of this thesis. Therefore, for future testing of the developed sensor in GCF measurement, a person having a body mass of around 55 kgs will be chosen.

The model building at 55psi was carried out in a similar way like before. Firstly, loading and unloading were done till 900N and the break point between region 2 and region 3 was noted. Linear models were approximated for region 1 and region 2 (Table 6). After that, mean of the models were taken (Table 7) by taking average of the two models. The third region was omitted in this case while doing the model building as shown in fig. 35. After finding out the best linear models, loading and unloading cycle was done till 690N and the performance of the developed model was determined as seen in fig. 36. It was found out the model showed good performance with RMSE of 24.0406N and 22.4289N for loading and unloading respectively and hence ideal for use in a 55 kg person.

Table 4: Model Building at 35psi

	Loading	**Unloading**
Region 1	$4.779\times x - 1837 (R^2 = 0.9769)$	$3.348\times - 1277 (R^2 = 0.972)$
Region 2	$2.684\times x - 973.5 (R^2 = 0.9983)$	$2.437\ \times x - 909.8 (R^2 = 0.9979)$
Region 3	$17.97\times x - 1.009e04 (R^2 = 0.857)$	$32.74\times x - 1.904e04 (R^2 = 0.8954)$

Table 5: Mean Model at 35psi

	Mean Model
Region 1	$4.0635\times - 1577$
Region 2	$2.5605\ \times x - 933.25$
Region 3	$25.355\times x - 14.4565e04$

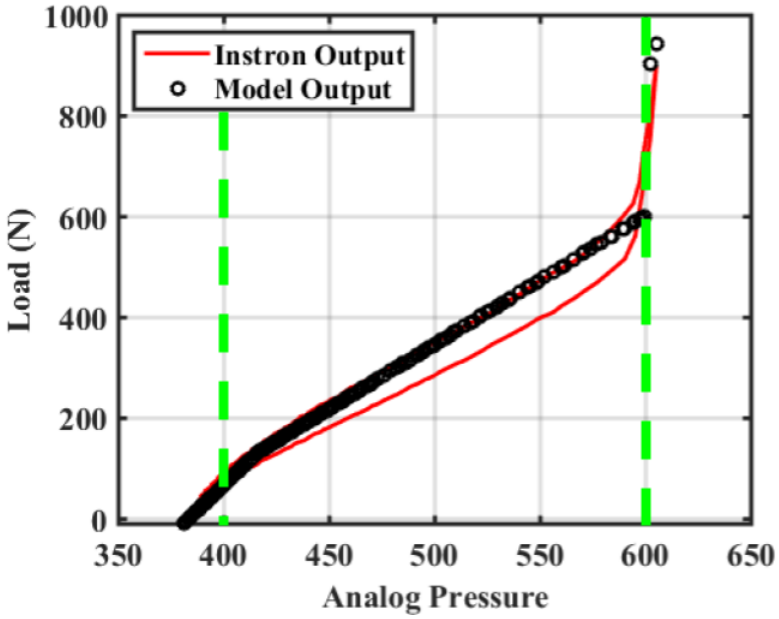

Figure 34: Model Validation at 35psi

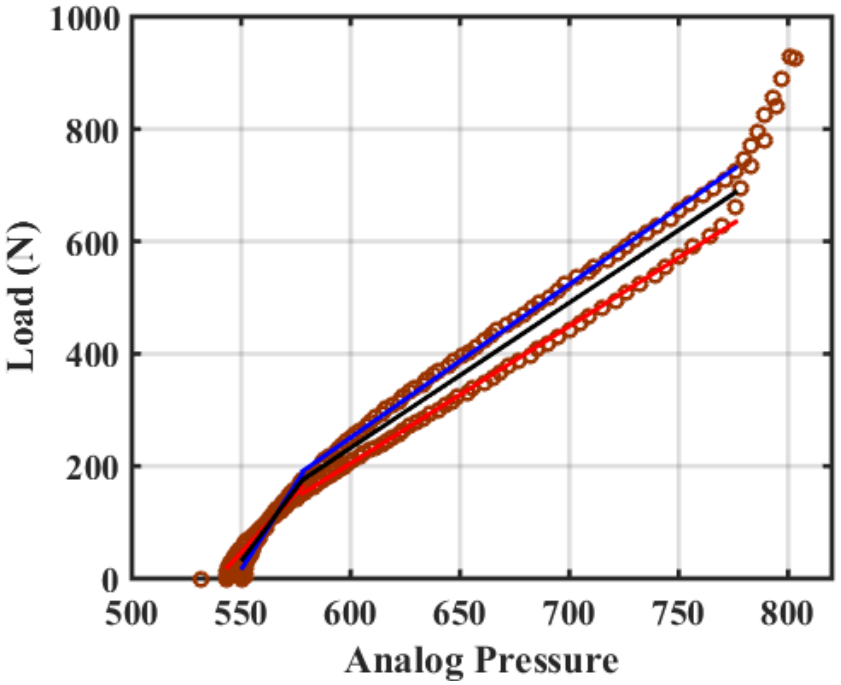

Figure 35: Model Building at 55psi

Table 6: Model Building at 55psi

	Loading	**Unloading**
Region 1	$6.107\times x - 3343 (R^2 = 0.9691)$	$4.201\times - 2264 (R^2 = 0.972)$
Region 2	$2.728\times x - 1386 (R^2 = 0.998)$	$2.443\ \times x - 1261 (R^2 = 0.9988)$

Table 7: Mean Model at 55psi

	Mean Model
Region 1	$5.154\times x - 2803.5$
Region 2	$2.5855\ \times x - 1318.9$

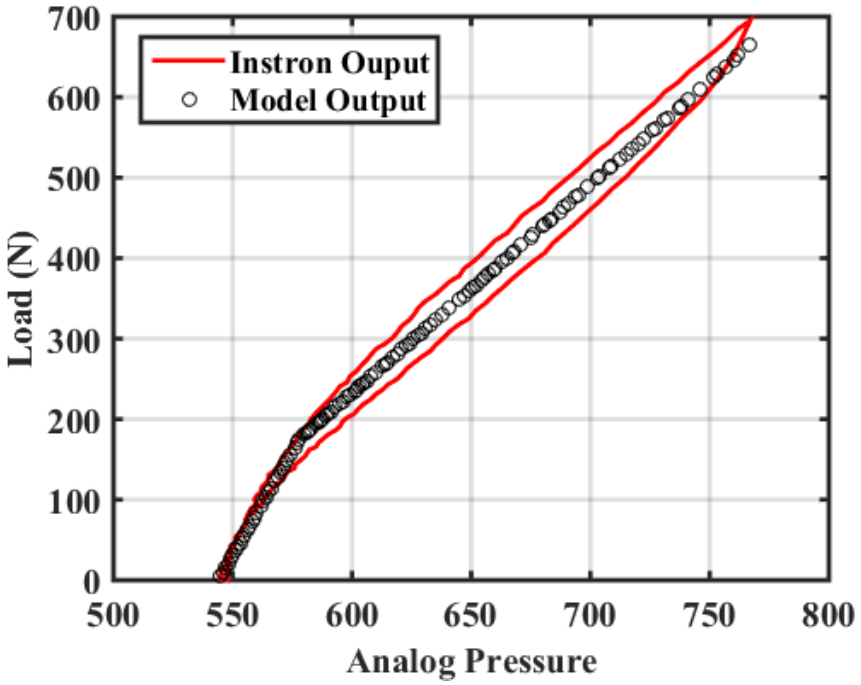

Figure 36: Model Validation at 55psi

4.5 Silicone Insole

In this work, insole was fabricated and designed according to the functional requirements specified in the beginning of the chapter. Silicone rubber was used to

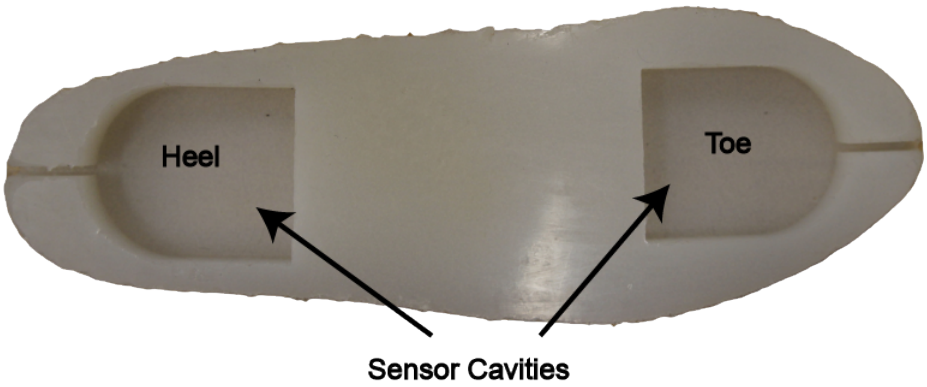

Figure 37: Silicone Insole

fabricate the insole to make it compliant and give comfort to the user. To fabricate the insole, dimensions of a size 9 insole were taken and a mould was 3D printed as shown in fig. 37. For creating cavities to place the insole sensors, rectangular boxes were 3D printed and placed in the areas of heel and toe respectively. Liquid Silicone was poured in the mould until it reached 15mm thickness and kept at 60 degree celsius inside an oven for an hour until it cured and hardened. The silicone insole was finally taken out of the mould.

4.6 Integration of Sensors in Insole and Electro-Pneumatics

Two sensors were fabricated and placed in the silicone insole in heel and toe areas respectively. Each balloon of the three chamber sensors were connected via four way plastic barbed connectors with the fourth way connecting the check valves to hold the air pressure inside. Each of the sensors were connected to two pressure sensors via three way plastic connectors. Arduino microcontroller was used to gather the force and pressure data from the sensors. Integration of shoe with a human subject is shown in fig. 38.

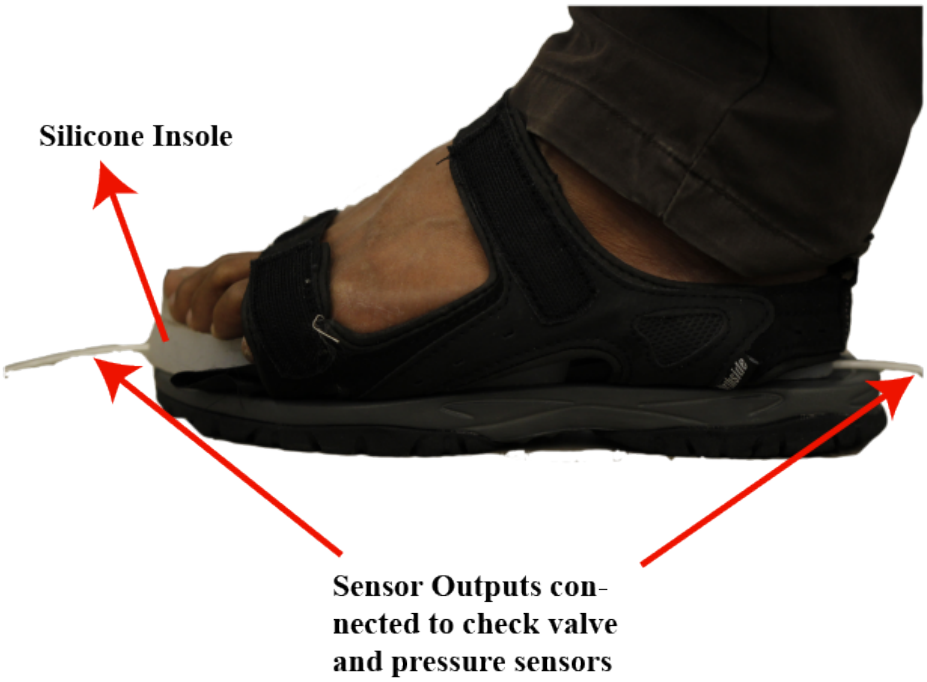

Figure 38: Integration of Shoe with Human Subject

Chapter 5

CHAPTER SUMMARY AND DISCUSSION

5.1 Chapter 1

This chapter gave a brief overview for the motivation of this thesis work. The initial portions talked about the need for rehabilitation and the importance of robotic devices which can reduce workload on physical therapists for carrying out rehabilitative tasks. The next portions talked about the importance of soft exosuits and its advantage over rigid exoskeletons. Motivation behind the use of less explored fabric based inflatable actuators for use in lower body exosuits was given. Since, current fabric based actuators used for lower limb rehabilitation have slow dynamics, use of actuator composite was proposed. The next sections talked about the limitations of the current portable wearable devices utilizing pneumatic supply which needs replacement and refilling of power source and also being heavy and bulky. Therefore, to make the exosuit device portable and light weight, a portable pneumatic source was decided to be developed. The last section talked about the importance of gait sensing in rehabilitation and gave a brief overview of the existing gait sensing methods which are mainly resistive, capacitive, inductive, fiber grating and pneumatic sensing. Motivation behind the use of inflatable sensors was also given.

5.2 Chapter 2

This chapter talked about using a novel actuator composite which can be used in exosuits for knee extension assistance. Such actuator composites can help in achieving faster actuation as compared to inflatable fabric beams. The first section talked about the design and fabrication of the actuator composite and also the motivation and need for composites. The IAC consists of 3D printed rigid paddles placed in series with that of the inflatable fabric layers. It was demonstrated through experiments that the IAC had similar performance like IFB even though the inflatable volume was minimized compared to that of the IFB. Next sections talked about building finite element models for the IFB and IAC. The procedure for building the finite element models was shown. They were further simulated in a quasi static manner in Abaqus/Explicit and the simulation results were verified with that of the experimental results. The simulation was done is a similar way as that of the experimental setup where boundary conditions and tie constraints were used in place of using clamps and sewing. The results showed a good match with an acceptable RMSE error of 6.33° and 4.63° for the IAC and IFB respectively. After model validation was carried out, optimization of the actuator volume was also done by taking inflatable section volume at 33%, 66% and 100%. It was determined that the performance of the composite remained same irrespective of the change in internal volume.

5.3 Chapter 3

This chapter talked about the fabrication and development of a portable pneumatic air source which can be mounted on a back- pack frame and carried by the user outside

laboratory confinements. This air source doesn't need refilling prior to use in wearable pneumatic applications unlike previous air sources and is compact because of its parallel arrangement. The type of mechanism used for working of the air source is lead screw based linear drive mechanism. In this mechanism, a DC motor drives a cylinder piston arrangement, all arranged in a parallel fashion. Parallel arrangement was chosen to account for system compactness and portability. Speed regulation for DC motor was done by means of DC brushed controller which operated via Pulse Width Modulation signals for controlling motor frequency. The completion of each stroke was determined by means of limit switches placed at two extremities of each stroke. Triggering of the limit switches caused changes in rotational direction of the DC motor and that's how different strokes were obtained. The whole system was controlled by a Raspberry Pi module. Pressurised output was obtained through check valves and switching solenoid valves for each consecutive stroke. The solenoid valves were controlled via a 4 channel MOSFET board. The Raspberry Pi and other controllers were placed one above the other by means of transparent acrylic sheets. The power source for the system was a 24V battery. A voltage regulator was used to supply 5V to the Raspberry Pi. Finally, evaluation of the system was done by checking the system's maximum pressure and flow output capabilities. It was concluded that the system is capable of generating a maximum pressure of 0.131 MPa and a flow rate of 21.45 SLPM.

5.4 Chapter 4

This chapter showed a novel way of gait sensing using fabric based inflatable sensors. Fabrication methodology of making leak proof sensors was shown which

eliminated the need for threaded connectors. In this type of fabrication technique, the tubing was directly put inside the sensor and two layers of hot glue were put all around it. Detailed procedure of design selection for the sensors was also shown. After a rigorous testing procedure, a triple balloon sensor design was chosen. Mechanical characterization of the developed sensor design was carried out. It was concluded that the sensor demonstrated good repeatability and also had rate independent hysteresis which is ideal for use in fast or slow paced walking scenarios. In this work, a silicone insole was fabricated by taking a standard insole size. Silicone was chosen to make it complaint to the user. Fabrication procedure of the Silicone insole was shown which involved making a 3D printed mould and pouring liquid silicone all over it. The mould containing the liquid Silicone when cured in an oven, became rubbery and soft. Provisions were made for placing the sensors by means of cavities carved inside the Silicone insole. Integration of two sensors in Heel and Toe area was also shown along with electro- pneumatics setup. Future use of the developed shoe in gait detection was also given.

Chapter 6

CONCLUSION AND FUTURE WORK

The purpose of this thesis was to make a soft portable exosuit for knee assistance which can be used for rehabilitative purposes. This work has focused on achieving faster actuator dynamics, system portability and gait sensing using soft inflatable chambers. The area of actuation mechanism in this work focused on achieving faster actuation and reduction in inflation work compared to inflatable fabric beam actuators used in previous versions of the exosuit. This was done by introducing inflatable actuator composites which had a reduced volume and the extra volume was replaced by using rigid paddles. Performance evaluation was done by means of experimental testing and building finite element models, concluding that the actuator performance was unaffected by reduction in internal volume. Given the drawbacks of current exosuit technologies which are mostly tethered and needs continuous recharge of the power source prior to usage, an air source was proposed which can be used in conjunction with inflatable actuators by mounting it on a back pack frame. The system worked by means of a linear drive system, powered by a DC motor. The air source is capable of generating pressure and flow output of 0.131 MPa and 21.45 SLPM, respectively. To generate an appropriate amount of knee assistance in various gait cycles through the actuator, gait feedback is needed. This work shows a novel way of gait sensing using soft inflatable fabric based sensors capable of detecting load of 700 N. The sensors are integrated into a shoe insole in heel and toe as a proof of concept.

In future, optimization of the design of the actuator composite will be done by finite element methods. Areas and cross sections will be varied to select the best

composite design. Force characteristics will be included in volume optimization to take into account the change in actuator weight when internal volumes are varied.

Efforts will also be put in reducing the overall weight of the portable system. Gearbox will be used with the DC motor to increase the pressure output. Additionally, vacuum generation capability will be explored which is necessary for achieving faster deflation.

Use of the developed shoe in various gait detection scenarios and its use in control of pneumatic wearable devices will be explored. Furthermore, force haptic feedback system will be included in shoe insole to help subjects in detecting abnormal gait. Additionally, robustnesss of the insole sensor will be increased by embedding it inside the silicone insole and placing the sensors in the insole mould and pouring liquid silicone all over it such that it encapsulates the whole sensor. In this way, the sensor can be made resistant to shocks which can make it prone to possible mechanical failures. The whole system will be made wireless and the electro-pneumatics setup will be embedded in shoe insole.

Furthermore, the design of the sensor will be optimized more to increase it's resolution and range of measurement which is currently limited to 700N. As per functional requirements of gait sensing, the sensor should measure a load of 900N. One possible way to increase the range of measurement is shown in fig. 39. It was seen from the flow chart of sensor design selection procedure (Fig. 21) and also from the sensor design optimization plots (Fig. 22), that the rectangular sensor of dimensions 70mm$\times$16mm could reach a payload capacity of 220N, however, the double chamber sensor with each chamber having half the length of the rectangular sensor and having similar volume overall has a payload capacity of 600N. This means, by cutting down the sensor into smaller pieces having similar overall volumes, larger

range of measurement can be obtained. Therefore, to increase the value of breakpoint of the triple balloon sensor design which currently saturates at 700N, the length of each balloon can be again cut into half and the two smaller balloons can be placed in series. By doing this, larger value of breakpoint of the sensor can be obtained. Fabrication of the proposed sensor design will be done in a similar way as that of the triple chamber sensor design with the new design requiring more number of chambers and hence, more number of TPU balloons and fabric sockets which might make it a bit of time consuming to fabricate. Time for fabrication can be reduced by using automated sewing instead of manual sewing and also, by using CNC machine for sealing the TPU layers.

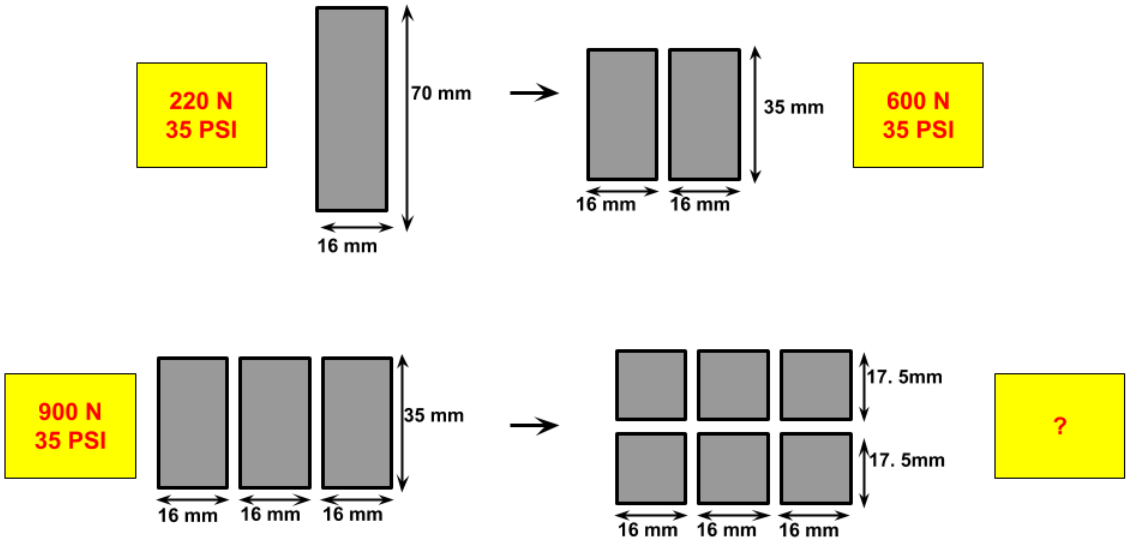

Figure 39: Sensor Design Enhancement

Finally, the IAC, the developed air source and the gait detection shoe will be used to make a portable soft exosuit for knee extension assistance. A recent work showed a similar integration of the IAC and the air source but with a different type of shoe

(also called smart shoes), utilizing coiled silicone tubings for sensing contact with the ground [63]. EMG evaluation was done showing reductions in muscle activity of the Vastus Literalis muscle group with the exosuit active. The next version of the soft exosuit will work on further development of the IAC, the air source and the newly developed shoe as mentioned in earlier paragraphs of this section. An upgraded exosuit will be developed utilizing these components and evaluation will be done by rigorous participant testing with the exosuit on.

REFERENCES

[1] Emelia J Benjamin, Paul Muntner, and Márcio Sommer Bittencourt. "Heart disease and stroke statistics-2019 update: a report from the American Heart Association." In: *Circulation* 139.10 (2019), e56–e528.

[2] Birol Balaban and Fatih Tok. "Gait disturbances in patients with stroke." In: *PM&R* 6.7 (2014), pp. 635–642.

[3] Sandra J Olney and Carol Richards. "Hemiparetic gait following stroke. Part I: Characteristics." In: *Gait & posture* 4.2 (1996), pp. 136–148.

[4] Peter Langhorne, Julie Bernhardt, and Gert Kwakkel. "Stroke rehabilitation." In: *The Lancet* 377.9778 (2011), pp. 1693–1702.

[5] Vernon Lin, Xiaoming Zhang, and Pamela Dixon. "Occupational therapy workforce in the United States: Forecasting nationwide shortages." In: *PM&R* 7.9 (2015), pp. 946–954.

[6] Mindy Lipson Aisen, H Igo Krebs, Neville Hogan, Fletcher McDowell, and Bruce T Volpe. "The effect of robot-assisted therapy and rehabilitative training on motor recovery following stroke." In: *Archives of neurology* 54.4 (1997), pp. 443–446.

[7] Daniel Sanz-Merodio, Manuel Cestari, Juan Carlos Arevalo, and Elena Garcia. "A lower-limb exoskeleton for gait assistance in quadriplegia." In: *2012 IEEE International Conference on Robotics and Biomimetics (ROBIO)*. IEEE. 2012, pp. 122–127.

[8] Manuel Cestari, Daniel Sanz-Merodio, Juan Carlos Arevalo, and Elena Garcia. "An adjustable compliant joint for lower-limb exoskeletons." In: *IEEE/ASME Transactions On Mechatronics* 20.2 (2014), pp. 889–898.

[9] Letian Wang, Shiqian Wang, Edwin HF van Asseldonk, and Herman van der Kooij. "Actively controlled lateral gait assistance in a lower limb exoskeleton." In: (2013), pp. 965–970.

[10] Ryan J Farris, Hugo A Quintero, and Michael Goldfarb. "Performance evaluation of a lower limb exoskeleton for stair ascent and descent with paraplegia." In: (2012), pp. 1908–1911.

[11] Conor James Walsh, Ken Endo, and Hugh Herr. "A quasi-passive leg exoskeleton for load-carrying augmentation." In: *International Journal of Humanoid Robotics* 4.03 (2007), pp. 487–506.

[12] C. J. Walsh, D. Paluska, K. Pasch, W. Grand, A. Valiente, and H. Herr. "Development of a lightweight, underactuated exoskeleton for load-carrying augmentation." In: (May 2006), pp. 3485–3491. DOI: 10.1109/ROBOT.2006.1642234.

[13] Zhiyong Tang, Di Shi, Difei Liu, Zhaoqin Peng, Longlong He, and Zhongcai Pei. "Electro-hydraulic servo system for Human Lower-limb Exoskeleton based on sliding mode variable structure control." In: (2013), pp. 559–563.

[14] Zhi Wang, Shiqiang Zhu, Qingcheng Chen, Xuequn Zhang, and Yang Song. "Sliding mode control of electro-hydraulic servo system for lower-limb exoskeleton based on RBF neural network." In: *2015 IEEE 10th Conference on Industrial Electronics and Applications (ICIEA)*. IEEE. 2015, pp. 79–83.

[15] Hongyue Hu, Kai Fang, Huanyi Guan, Xinyu Wu, and Chunjie Chen. "A Novel Control Method of A Soft Exosuit with Plantar Pressure Sensors." In: (2019), pp. 581–586.

[16] Alan T Asbeck, Stefano MM De Rossi, Kenneth G Holt, and Conor J Walsh. "A biologically inspired soft exosuit for walking assistance." In: *The International Journal of Robotics Research* 34.6 (2015), pp. 744–762.

[17] Louis N Awad, Jaehyun Bae, Kathleen O'donnell, Stefano MM De Rossi, Kathryn Hendron, Lizeth H Sloot, Pawel Kudzia, Stephen Allen, Kenneth G Holt, Terry D Ellis, et al. "A soft robotic exosuit improves walking in patients after stroke." In: *Science translational medicine* 9.400 (2017), eaai9084.

[18] Alan T Asbeck, Robert J Dyer, Arnar F Larusson, and Conor J Walsh. "Biologically-inspired soft exosuit." In: (2013), pp. 1–8.

[19] Alan T Asbeck, Kai Schmidt, Ignacio Galiana, Diana Wagner, and Conor J Walsh. "Multi-joint soft exosuit for gait assistance." In: *2015 IEEE International Conference on Robotics and Automation (ICRA)*. IEEE. 2015, pp. 6197–6204.

[20] Louis N Awad, Jaehyun Bae, Pawel Kudzia, Andrew Long, Kathryn Hendron, Kenneth G Holt, Kathleen O'Donnell, Terry D Ellis, and Conor J Walsh. "Reducing circumduction and hip hiking during hemiparetic walking through targeted assistance of the paretic limb using a soft robotic exosuit." In: *American journal of physical medicine & rehabilitation* 96.10 (2017), S157–S164.

[21] Carly M Thalman, Quoc P Lam, Pham H Nguyen, Saivimal Sridar, and Panagiotis Polygerinos. "A novel soft elbow exosuit to supplement bicep lifting capacity." In: (2018), pp. 6965–6971.

[22] Saivimal Sridar, Pham H Nguyen, Mengjia Zhu, Quoc P Lam, and Panagiotis Polygerinos. "Development of a soft-inflatable exosuit for knee rehabilitation." In: *2017 IEEE/RSJ International Conference on Intelligent Robots and Systems (IROS)*. IEEE. 2017, pp. 3722–3727.

[23] Saivimal Sridar, Zhi Qiao, Niveditha Muthukrishnan, Wenlong Zhang, and Panagiotis Polygerinos. "A soft-inflatable exosuit for knee rehabilitation: Assisting swing phase during walking." In: *Frontiers in Robotics and AI* 5 (2018), p. 44.

[24] Yong-Lae Park, Jobim Santos, Kevin G Galloway, Eugene C Goldfield, and Robert J Wood. "A soft wearable robotic device for active knee motions using flat pneumatic artificial muscles." In: (2014), pp. 4805–4810.

[25] Takahiro Kanno, Daisuke Morisaki, Ryoken Miyazaki, Gen Endo, and Kenji Kawashima. "A walking assistive device with intention detection using back-driven pneumatic artificial muscles." In: (2015), pp. 565–570.

[26] Shilong Wan, Mingxing Yang, Ruru Xi, Xingsong Wang, Ruiming Qian, and Qingcong Wu. "Design and control strategy of humanoid lower limb exoskeleton driven by pneumatic artificial muscles." In: *2016 23rd International Conference on Mechatronics and Machine Vision in Practice (M2VIP)*. IEEE. 2016, pp. 1–5.

[27] Michael Wehner, Michael T Tolley, Yiğit Mengüç, Yong-Lae Park, Annan Mozeika, Ye Ding, Cagdas Onal, Robert F Shepherd, George M Whitesides, and Robert J Wood. "Pneumatic energy sources for autonomous and wearable soft robotics." In: *Soft robotics* 1.4 (2014), pp. 263–274.

[28] Haifan Wu, Ato Kitagawa, Hideyuki Tsukagoshi, and Canghai Liu. "Development of a novel pneumatic power assisted lower limb for outdoor walking by the use of a portable pneumatic power source." In: (2007), pp. 1291–1296.

[29] Manabu Okui, Yuki Nagura, Yasuyuki Yamada, and Taro Nakamura. "Hybrid pneumatic source based on evaluation of air compression methods for portability." In: *IEEE Robotics and Automation Letters* 3.2 (2018), pp. 819–826.

[30] Michael Wehner, Brendan Quinlivan, Patrick M Aubin, Ernesto Martinez-Villalpando, Michael Baumann, Leia Stirling, Kenneth Holt, Robert Wood, and Conor Walsh. "A lightweight soft exosuit for gait assistance." In: (2013), pp. 3362–3369.

[31] Chetan Thakur, Kazunori Ogawa, Toshio Tsuji, and Yuichi Kurita. "Soft wearable augmented walking suit with pneumatic gel muscles and stance phase detection system to assist gait." In: *IEEE Robotics and Automation Letters* 3.4 (2018), pp. 4257–4264.

[32] Ryeonho Kang, Ho Seon Choi, and Yoon Su Baek. "Design of a Portable Radial Piston Pneumatic Compressor for Wearable Robot System." In: (2018), pp. 86–89.

[33] Sangjoon J Kim, Handdeut Chang, Junghoon Park, and Jung Kim. "Design of a Portable Pneumatic Power Source With High Output Pressure for Wearable Robotic Applications." In: *IEEE Robotics and Automation Letters* 3.4 (2018), pp. 4351–4358.

[34] Kamen Ivanov, Zhanyong Mei, Ludwig Lubich, Nan Guo, Deng Xile, Zhichun Zhao, Olatunji Mumini Omisore, Derek Ho, and Lei Wang. "Design of a Sensor Insole for Gait Analysis." In: (2019), pp. 433–444.

[35] SMM De Rossi, Tommaso Lenzi, Nicola Vitiello, Marco Donati, Alessandro Persichetti, Francesco Giovacchini, Fabrizio Vecchi, and Maria Chiara Carrozza. "Development of an in-shoe pressure-sensitive device for gait analysis." In: (2011), pp. 5637–5640.

[36] Simona Crea, Marco Donati, Stefano Marco Maria De Rossi, Calogero Maria Oddo, and Nicola Vitiello. "A wireless flexible sensorized insole for gait analysis." In: *Sensors* 14.1 (2014), pp. 1073–1093.

[37] Lin Shu, Tao Hua, Yangyong Wang, Qiao Li, David Dagan Feng, and Xiaoming Tao. "In-shoe plantar pressure measurement and analysis system based on fabric pressure sensing array." In: *IEEE Transactions on information technology in biomedicine* 14.3 (2010), pp. 767–775.

[38] Jin Huat Low, Phone May Khin, and Chen-Hua Yeow. "A pressure-redistributing insole using soft sensors and actuators." In: (2015), pp. 2926–2930.

[39] Wenzheng Heng, Gaoyang Pang, Feihong Xu, Xiaoyan Huang, Zhibo Pang, and Geng Yang. "Flexible Insole Sensors with Stably Connected Electrodes for Gait Phase Detection." In: *Sensors* 19.23 (2019), p. 5197.

[40] Jiaxin Wan, Qi Wang, Siyao Zang, Tao Wang, Guoqing Liu, Chunsheng Li, Xiaomin Ren, et al. "Highly stretchable and sensitive liquid-type strain sensor based on a porous elastic rope/elastomer matrix composite structure." In: *Composites Science and Technology* 182 (2019), p. 107707.

[41] Xiaoshuang Duan, Yanbo Yao, Muchuan Niu, Jiangjiang Luo, Rui Wang, and Tao Liu. "Direct Laser Writing of Functional Strain Sensors in Polyimide Tubes." In: *ACS Applied Polymer Materials* 1.11 (2019), pp. 2914–2923.

[42] Pablo Aqueveque, Enrique Germany, Rodrigo Osorio, and Francisco Pastene. "Gait Segmentation Method Using a Plantar Pressure Measurement System with Custom-Made Capacitive Sensors." In: *Sensors* 20.3 (2020), p. 656.

[43] Ines Sorrentino, Francisco Javier Andrade Chavez, Claudia Latella, Luca Fiorio, Silvio Traversaro, Lorenzo Rapetti, Yeshasvi Tirupachuri, Nuno Guedelha, Marco Maggiali, Simeone Dussoni, et al. "A Novel Sensorised Insole for Sensing Feet Pressure Distributions." In: *Sensors* 20.3 (2020), p. 747.

[44] Vivek Chandel, Shivam Singhal, Varsha Sharma, Nasimuddin Ahmed, and Avik Ghose. "PI-Sole: A Low-Cost Solution for Gait Monitoring Using Off-The-Shelf Piezoelectric Sensors and IMU." In: *2019 41st Annual International Conference of the IEEE Engineering in Medicine and Biology Society (EMBC)*. IEEE. 2019, pp. 3290–3296.

[45] Qi Zhang, Yu Lu Wang, Yun Xia, Xuee Wu, Timothy Vernon Kirk, and Xiao Dong Chen. "A low-cost and highly integrated sensing insole for plantar pressure measurement." In: *Sensing and Bio-Sensing Research* 26 (2019), p. 100298.

[46] Changwon Wang, Young Kim, Hangsik Shin, and Se Dong Min. "Preliminary Clinical Application of Textile Insole Sensor for Hemiparetic Gait Pattern Analysis." In: *Sensors* 19.18 (2019), p. 3950.

[47] Wei Wang, Junyi Cao, Jian Yu, Rong Liu, Chris R Bowen, and Wei-Hsin Liao. "Self-Powered Smart Insole for Monitoring Human Gait Signals." In: *Sensors* 19.24 (2019), p. 5336.

[48] Suryakanta Nayak, Yida Li, Willie Tay, Evgeny Zamburg, Devendra Singh, Chengkuo Lee, Soo Jin Adrian Koh, Patrick Chia, and Aaron Voon-Yew Thean. "Liquid-metal-elastomer foam for moldable multi-functional triboelectric energy harvesting and force sensing." In: *Nano Energy* 64 (2019), p. 103912.

[49] Baoqing Nie, Rong Huang, Ting Yao, Yiqiu Zhang, Yihui Miao, Changrong Liu, Jian Liu, and Xinjian Chen. "Textile-Based Wireless Pressure Sensor Array for Human-Interactive Sensing." In: *Advanced Functional Materials* 29.22 (2019), p. 1808786.

[50] Rafique Ahmed Lakho, Zhang Yi-Fan, Jiang Jin-Hua, Hong Cheng-Yu, and Zamir Ahmed Abro. "A smart insole for monitoring plantar pressure based on

the fiber Bragg grating sensing technique." In: *Textile Research Journal* 89.17 (2019), pp. 3433–3446.

[51] Kyoungchul Kong and Masayoshi Tomizuka. "A gait monitoring system based on air pressure sensors embedded in a shoe." In: *IEEE/ASME Transactions on mechatronics* 14.3 (2009), pp. 358–370.

[52] Wenlong Zhang, Masayoshi Tomizuka, and Nancy Byl. "A wireless human motion monitoring system for smart rehabilitation." In: *Journal of Dynamic Systems, Measurement, and Control* 138.11 (2016).

[53] Liangliang Wang and Zheng Wang. "Mechanoreception for Soft Robots via Intuitive Body Cues." In: *Soft robotics* (2019).

[54] Daoxiong Gong, Rui He, Jianjun Yu, and Guoyu Zuo. "A pneumatic tactile sensor for co-operative robots." In: *Sensors* 17.11 (2017), p. 2592.

[55] Hyunjin Choi and Kyoungchul Kong. "A Soft Three-Axis Force Sensor Based on Radially Symmetric Pneumatic Chambers." In: *IEEE Sensors Journal* 19.13 (2019), pp. 5229–5238.

[56] Hui Yang, Yang Chen, Yao Sun, and Lina Hao. "A novel pneumatic soft sensor for measuring contact force and curvature of a soft gripper." In: *Sensors and Actuators A: Physical* 266 (2017), pp. 318–327.

[57] Jaewoong Jung, Myungsun Park, Dong Wook Kim, and Yong-Lae Park. "Optically Sensorized Elastomer Air Chamber for Proprioceptive Sensing of Soft Pneumatic Actuators." In: *IEEE Robotics and Automation Letters* (2020).

[58] Yang Chen, Shaofei Guo, Cunfeng Li, Hui Yang, and Lina Hao. "Size recognition and adaptive grasping using an integration of actuating and sensing soft pneumatic gripper." In: *Robotics and Autonomous Systems* 104 (2018), pp. 14–24.

[59] Stefan Escaida Navarro, Olivier Goury, Gang Zheng, Thor Morales Bieze, and Christian Duriez. "Modeling Novel Soft Mechanosensors based on Air-Flow Measurements." In: *IEEE Robotics and Automation Letters* 4.4 (2019), pp. 4338–4345.

[60] Sunny Amatya, Amir Salimi Lafmejani, Souvik Poddar, Saivimal Sridar, Thomas Sugar, and Panagiotis Polygerinos. "Design, Development, and Control of a Fabric-Based Soft Ankle Module to Mimic Human Ankle Stiffness." In: (2019), pp. 886–891.

[61] JP Pollard, LP Le Quesne, and JW Tappin. "Forces under the foot." In: *Journal of biomedical engineering* 5.1 (1983), pp. 37–40.

[62] Pham H Nguyen, IB Imran Mohd, Curtis Sparks, Francisco L Arellano, Wenlong Zhang, and Panagiotis Polygerinos. "Fabric soft poly-limbs for physical assistance of daily living tasks." In: *2019 International Conference on Robotics and Automation (ICRA)*. IEEE. 2019, pp. 8429–8435.

[63] S. Sridar, S. Poddar, Y. Tong, P. Polygerinos, and W. Zhang. "Towards Untethered Soft Pneumatic Exosuits using Low-Volume Inflatable Actuator Composites and a Portable Pneumatic Source." In: *IEEE Robotics and Automation Letters* (2020), pp. 1–1.